1525

1525

NACA

RESEARCH MEMORANDUM

TESTS IN THE AMES 40- BY 80-FOOT WIND TUNNEL OF AN AIRPLANE

CONFIGURATION WITH AN ASPECT RATIO 3 TRIANGULAR WING

AND AN ALL-MOVABLE HORIZONTAL TAIL - LONGITUDINAL

AND LATERAL CHARACTERISTICS

By David G. Koenig

Ames Aeronautical Laboratory
Moffett Field, Calif.

NATIONAL ADVISORY COMMITTEE
FOR AERONAUTICS
WASHINGTON

April 13, 1953

NATIONAL ADVISORY COMMITTEE FOR AERONAUTICS

RESEARCH MEMORANDUM

TESTS IN THE AMES 40- BY 80-FOOT WIND TUNNEL OF AN AIRPLANE

CONFIGURATION WITH AN ASPECT RATIO 3 TRIANGULAR WING

AND AN ALL-MOVABLE HORIZONTAL TAIL - LONGITUDINAL

AND LATERAL CHARACTERISTICS

By David G. Koenig

SUMMARY

An investigation has been made to determine the low-speed large-scale characteristics of an aspect ratio 3 triangular-wing airplane model. The complete model consisted of the wing in combination with a fuselage of fineness ratio 12.5; a thin, triangular vertical tail with a constant-chord rudder; and a thin, unswept, all-movable tail (aspect ratio of approximately 4). The wing had an NACA 0005 (modified) section and was equipped with partial-span, slotted, trailing-edge flaps of constant chord. Tests of the model at zero sideslip were made with the horizontal tail at each of three vertical positions (0, 0.21, and 0.41 wing semispan above the extended wing-chord plane) at one fixed longitudinal distance behind the wing. The characteristics of the model in sideslip were investigated with the tail in the extended wing-chord plane. In addition, a limited investigation was made on the use of flaps or the horizontal tail as a lateral-control device. The average Reynolds number, based on the wing mean aerodynamic chord, was 12.8 million and the Mach number was 0.13.

INTRODUCTION

Wind-tunnel tests at subsonic and supersonic speeds have been made for small-scale, aspect ratio 3 triangular wings. In order to extend the scope of data on the aspect ratio 3 triangular-wing plan form to that of large scale, an investigation has been conducted in the Ames 40- by 80-foot wind tunnel.

For purposes of paralleling previous investigations of airplane configurations with aspect ratios 2 and 4 triangular wings in the 40- by 80-foot wind tunnel (refs. 1, 2, and 3), an aspect ratio 3 triangular wing with an NACA 0005 (modified) section equipped with trailing-edge partial-span slotted flaps of constant chord was tested in combination with a fuselage, vertical tail, and horizontal tail. This combination was identical to that used in the previous investigations. In addition to symmetrical control deflections, the flaps and horizontal tail were deflected asymmetrically and a limited investigation of their use as lateral-control devices was made.

The results are presented herein without analysis in order to expedite publication.

NOTATION

Figure 1 shows the sign convention used for presentation of the data. All control-surface deflections are measured in a plane perpendicular to the hinge or pivot line of the control surface.

b wing span, ft

b_f wing-flap span (movable), ft

b_t horizontal-tail span, ft

c wing chord, measured parallel to wing center line, ft

$\bar{c}$ mean aerodynamic chord of wing, measured parallel to wing

$$\text{center line,} \quad \frac{\int_0^{b/2} c^2 dy}{\int_0^{b/2} c\, dy}, \text{ ft}$$

C_D drag coefficient, drag/qS

C_l rolling-moment coefficient, rolling moment/qSb

C_L lift coefficient, lift/qS

C_m pitching-moment coefficient, pitching moment/$qS\bar{c}$

C_n yawing-moment coefficient, yawing moment/qSb

C_Y side-force coefficient, side force/qS

D   total drag, lb

i_t horizontal-tail incidence relative to the wing-chord plane, deg

l_t distance from moment center to pivot line of the horizontal
         tail, ft

L   total lift, lb

L/D   lift-drag ratio

p   rate of rolling, radians/sec

pb/2V   wing-tip helix angle, radians

q   free-stream dynamic pressure, lb/sq ft

S   wing area, sq ft

S_f trailing-edge-flap area (total movable), sq ft

S_t horizontal-tail area, sq ft

V   free-stream velocity, ft/sec

x   longitudinal coordinate parallel to model center line, ft

y   lateral coordinate perpendicular to plane of symmetry, ft

z   vertical coordinate perpendicular to wing-chord plane, ft

α angle of attack of the wing-chord plane with reference to free
         stream, deg

α_δ rate of change of wing-section angle of attack with control-
         surface angle for constant section lift

β angle of sideslip of the model plane of symmetry with reference
         to free stream, deg

δ_f average flap deflection with reference to the wing-chord plane,
         deg

δ_l difference in deflection between a pair of control surfaces used
         as lateral controls, positive when left-hand control has more
         positive deflection, deg
         (Sub-subscripts denote the control used: f, flaps; t, hori-
         zontal tail.)

δ_r rudder deflection, deg

ϵ_{av} average effective downwash, deg

C_{l_p} $\dfrac{\partial C_l}{\partial (pb/2V)}$

C_{l_β} $\left(\dfrac{\partial C_l}{\partial \beta}\right)_{\beta=0}$

C_{n_β} $\left(\dfrac{\partial C_n}{\partial \beta}\right)_{\beta=0}$

C_{Y_β} $\left(\dfrac{\partial C_Y}{\partial \beta}\right)_{\beta=0}$

DESCRIPTION OF MODEL

Pertinent geometric data are presented in table I and figure 2, and a photograph of the model is shown in figure 3.

The wing had an actual aspect ratio of 2.99 and NACA 0005 (modified) sections parallel to the model center line. The modification to the NACA 0005 sections consisted of a straight line fairing from the 67-percent-chord station to the trailing edge. The ordinates of the NACA 0005 (modified) section are presented in table II.

Because of the construction techniques used for the model, the ordinates of the actual wing section on a portion of the wing plan form were less than the ordinates of the NACA 0005 (modified) section by an amount not exceeding 0.1 percent of the local wing chord. The area on the wing plan form for which this deviation existed is shown in figure 4.

The wing was equipped with partial-span constant-chord slotted flaps which extended from 14.8 to 76.9 percent of the wing semispan. Dimensional data concerning the flap and slot profile are presented in figure 5.

The fuselage, vertical-tail, and horizontal-tail configuration was identical to that described in reference 1. The fuselage coordinates are listed in table III. A constant-chord rudder was installed on the vertical tail and had a plain radius nose and a small, unsealed gap.

The horizontal tail was installed at each of three vertical positions $(z/(b/2)$, of 0, 0.21, and 0.41 from the wing-chord plane). Hereafter, these tail positions will be referred to as low, middle, and high positions, respectively.

TESTS

Longitudinal characteristics were obtained with the model at zero sideslip. Tests were made with the horizontal tail off and with the tail installed in the low, middle, and high positions for various tail incidences. Tests were also made with the tail in the low position for a flap deflection of 40°. For purposes of aiding in the comparison of the longitudinal characteristics of the model with the horizontal tail at each of the tail positions, moment center locations were chosen such that a value of $(dC_m/dC_L)_{C_L=0} = -0.06$ would be obtained with the flaps and the horizontal tail undeflected. These moment centers were located at 43.6, 44.1, and 48.5 percent of the mean aerodynamic chord for the low, middle, and high positions, respectively.

The characteristics of the model in sideslip were investigated by making tests with varying angle of attack at 6° and 12° sideslip, and with varying angles of sideslip for 0°, 6°, 12°, 18°, and 24° angle of attack (nominal values). Sideslip data were obtained with the tail off and with the tail installed in the low position for flap deflections of 0° and 40°. For all sideslip data, a moment center location of 43.6 percent $\bar{c}$ was used.

Two means of lateral control were given a limited investigation, namely, asymmetrically deflected trailing-edge flaps and horizontal tail. The investigation was primarily concerned with lateral-control effectiveness at high trim lift coefficients. Tests were made with the complete model and with the horizontal tail off in order to determine the effect of the tail on the lateral-control effectiveness of the flaps.

In order to evaluate the effectiveness of the rudder and to determine the magnitude of the lateral-directional control interference, between the rudder and the horizontal tail, tests were made with the rudder deflected in combination with either a symmetrical or an asymmetrical deflection of the horizontal tail.

The data were corrected for wind-tunnel-wall effects and support-strut interference.

The Reynolds number of the tests was 12.8 million. The dynamic pressure was approximately 25 pounds per square foot and the Mach number was 0.13.

RESULTS

A summary of the configurations investigated is presented in table IV which also serves as an index to the basic aerodynamic data presented in figures 6 through 20.

A comparison of lift, drag, and pitching-moment characteristics of the wing-fuselage vertical-tail combination with those predicted by the theory of reference 4 for the wing alone is presented in figure 21.

The variation of ΔC_L due to 40° flap deflection with α is given in figure 22. In addition, the variation of ΔC_L as predicted by reference 5 is presented. Values of α_δ used in the computations were obtained from the curve of figure 3, reference 5, for the case of the gap sealed and a flap deflection range of 0° to 20°. Computations of ΔC_L were based on the span of the flap actually deflected.

The effect of tail height on the longitudinal-stability characteristics of the model is presented in figure 23. The variation of the average effective downwash with angle of attack is presented in figure 24 to show the source of the effect of tail height on the longitudinal stability of the model. The downwash data were derived by using the pitching-moment curves of figures 6, 7, and 8. The values were determined by the relation, $\epsilon_{av} = \alpha + i_t$, where α is the angle of attack at which the tail-on and tail-off pitching-moment curves intersected. In order to obtain points of intersection for tail incidences other than those tested, a linear variation of dC_m/di_t was assumed. This assumption is substantiated by the data of figure 9.

The trim lift and drag characteristics for the model with the horizontal tail at the low position are presented in figure 25. These trim data were derived from the data of figure 9. Curves of constant gliding and sinking speed based on a wing loading of 30 pounds per square foot are superimposed on the drag curves of figure 25.

The derivatives C_{l_β}, C_{n_β}, and C_{Y_β} are presented in figure 26 for the model with the horizontal tail off and on, for flap deflections of 0° and 40°. The values were obtained from the data of figures 11, 13, and 15 for the condition of zero sideslip.

The increments of C_l, C_n, and C_Y per degree of total lateral-control deflection of the flaps and of the horizontal tail are presented in figures 27 and 28, respectively. The rolling effectiveness of both lateral-control devices as predicted by the theory of reference 6 is also presented in figures 27 and 28. Values of $pb/2V$ for

each type of lateral control deflected to $\delta_l = 10^\circ$ are given in figure 29. Values of C_{l_p} were obtained from the experimental data in reference 7 for an aspect ratio 3 triangular-wing-alone model. Values of $pb/2V$ were obtained by dividing the experimental increments of rolling moment for a total aileron deflection of 10° by corresponding values of C_{l_p} as obtained from reference 10.

The increments of C_l, C_n, and C_Y per degree of rudder deflection for the complete model at zero sideslip are presented in figure 30. The increments shown are for differential deflections of 0° and 20° of the horizontal tail.

Ames Aeronautical Laboratory,
    National Advisory Committee for Aeronautics,
        Moffett Field, Calif.

REFERENCES

1. Graham, David, and Koenig, David G.: Tests in the Ames 40- by 80-Foot Wind Tunnel of an Airplane Configuration With an Aspect Ratio 2 Triangular Wing and an All-Movable Horizontal Tail - Longitudinal Characteristics. NACA RM A51B21, 1951.

2. Graham, David, and Koenig, David G.: Tests in the Ames 40- by 80-Foot Wind Tunnel of an Airplane Configuration With an Aspect Ratio 2 Triangular Wing and an All-Movable Horizontal Tail - Lateral Characteristics. NACA RM A51L03, 1952.

3. Graham, David, and Koenig, David G.: Tests in the Ames 40- by 80-Foot Wind Tunnel of an Airplane Configuration With an Aspect Ratio 4 Triangular Wing and an All-Movable Horizontal Tail - Longitudinal Characteristics. NACA RM A51H10a, 1951.

4. DeYoung, John, and Harper, Charles W.: Theoretical Symmetric Span Loading at Subsonic Speeds for Wings having Arbitrary Plan Form. NACA Rep. 921, 1948.

5. DeYoung, John: Theoretical Symmetric Span Loading Due to Flap Deflection for Wings of Arbitrary Plan Form at Subsonic Speeds. NACA Rep. 1071, 1951. (Supersedes NACA TN 2278)

6. DeYoung, John: Theoretical Antisymmetric Span Loading for Wings of
      Arbitrary Plan Form at Subsonic Speeds. NACA Rep. 1056, 1951.
      (Supersedes NACA TN 2140)

7. Tosti, Louis R.: Low-Speed Static Stability and Damping-in-Roll
      Characteristics of Some Swept and Unswept Low-Aspect-Ratio Wings.
      NACA TN 1468, 1947.

TABLE I.- GEOMETRIC DATA

Wing

Area, sq ft 313.76
Span, ft 30.64
Mean aerodynamic chord, ft 13.65
Aspect ratio 2.99
Taper ratio 0
Airfoil section parallel to model
  center line . . . . NACA 0005 (modified)

Fuselage

Length, ft 56.16
Maximum diameter, ft 4.49
Fineness ratio 12.5

Vertical tail

Exposed area, sq ft 52.53
Aspect ratio of plan form, extended
  to model center line 1
Taper ratio 0
Airfoil section parallel to model
  center line . . . . NACA 0005 (modified)
Rudder area (exposed), sq ft   12.87

Slotted, trailing-edge flaps

Chord (percent wing chord at fuselage
  center line) 9.57
S_f/S (total movable) 0.119
b_f/b (total movable) 0.622

Horizontal tail

Low position

S_t/S 0.245
b_t/b 0.602
$l_t/\bar{c}$ (moment center at $0.436\bar{c}$) 1.550
Aspect ratio 4.4
Taper ratio 0.46
$z/(b/2)$ 0

TABLE I.- GEOMETRIC DATA - Concluded

Middle position

S_t/S 0.199
b_t/b 0.495
$l_t/\bar{c}$ (moment center at $0.441\bar{c}$) 1.544
Aspect ratio 4.0
Taper ratio 0.50
$z/(b/2)$ 0.21

High position

S_t/S 0.199
b_t/b 0.495
$l_t/\bar{c}$ (moment center at $0.485\bar{c}$) 1.501
Aspect ratio 4.0
Taper ratio 0.50
$z/(b/2)$ 0.41

NACA

TABLE II.- COORDINATES OF THE NACA 0005
(MODIFIED) SECTION

Station (Percent chord)	Ordinate (Percent chord)
0	0
1.25	.789
2.50	1.089
5.00	1.481
7.50	1.750
10.00	1.951
15.00	2.228
20.00	2.391
25.00	2.476
30.00	2.501
40.00	2.419
50.00	2.206
60.00	1.902
67.00	1.650
70.00	1.500
80.00	1.000
90.00	.500
100.00	0

L.E. radius: 0.275-percent chord

TABLE III.- BODY COORDINATES

[Stations and radii in percent
of the total length]

Station		Radius
0	100.00	0
.625	99.38	.26
1.25	98.75	.42
2.50	97.50	.70
5.00	95.00	1.15
7.50	92.50	1.54
10.00	90.00	1.86
15.00	85.00	2.41
20.00	80.00	2.86
25.00	75.00	3.22
30.00	70.00	3.51
35.00	65.00	3.73
40.00	60.00	3.88
45.00	55.00	3.97
50.00	- - -	4.00

~NACA~

TABLE IV.- SUMMARY OF CONFIGURATIONS INVESTIGATED

[W, wing; F, fuselage; V, vertical tail; HL, HM, HH, horizontal tail at low, middle, and high positions, respectively]

Figure	Configuration	Control deflection, deg					β deg	α deg (nominal)	Data
		δ_f	δ_{l_f}	i_t	δ_{l_t}	δ_r			
6	W+F+V and W+F+V+HL	0, 40	0	tail off 0, -6	0	0	0	-2 to 25	C_L vs α, C_D, C_m
7	W+F+V and W+F+V+HM	0	0	tail off 0, -6	0	0	0	-2 to 25	C_L vs α, C_D, C_m
8	W+F+V and W+F+V+HH	0	0	tail off 0, -6	0	0.	0	-2 to 25	C_L vs α, C_D, C_m
9(a), (b)	W+F+V+HL	0, 40	0	2 to -10	0	0	0	-2 to 25	C_L vs α, C_D, C_m
10(a), (b)	W+F+V	0, 40	0	tail off		0	0,6,12	-2 to 25	C_L vs α, C_D, C_m, C_l, C_n, C_Y
11(a), (b), (c)	W+F+V	0, 40	0	tail off		0	-2 to 12	0,6,12,18, 24	C_L, C_D, C_m, C_l, C_n, C_Y vs β
12(a), (b)	W+F+V+HL	0	0	0	0	0	0,6,12	-2 to 25	C_L vs α, C_D, C_m, C_l, C_n, C_Y
13(a), (b) (c)	W+F+V+HL	0	0	0	0	0	-2 to 12	0,6,12,18, 24	C_L, C_D, C_m, C_l, C_n, C_Y vs β
14(a), (b)	W+F+V+HL	40	0	-6	0	0	0,6,12	-2 to 25	C_L vs α, C_D, C_m, C_l, C_n, C_Y
15(a), (b), (c)	W+F+V+HL	40	0	-6	0	0	-2 to 12	0,6,12,18, 24	C_L, C_D, C_m, C_l, C_n, C_Y vs β
16(a), (b)	W+F+V and W+F+V+HL	0 / 30	20 / 20	tail off -6	0	0	0	-2 to 25	C_L vs α, C_D, C_m, C_l, C_n, C_Y
17(a), (b), (c)	W+F+V and W+F+V+HL	30	20	tail off -6	0	0	-2 to 12	0,6,12,18, 24	C_L, C_D, C_m, C_l, C_n, C_Y vs β
18(a), (b)	W+F+V+HL	0 / 40	0	-6 / -6	0 / 20	0	0	-2 to 25	C_L vs α, C_D, C_m, C_l, C_n, C_Y
19(a), (b)	W+F+V+HL	40	0	-6 / -6	0 / 20	0,10 / 0,10	0	-2 to 25	C_L vs α, C_D, C_m, C_l, C_n, C_Y
20(a), (b), (c)	W+F+V+HL	40	0	-6 / -6	0 / 20	10	-2 to 12	0,6,12,18, 24	C_L, C_D, C_m, C_l, C_n, C_Y vs β
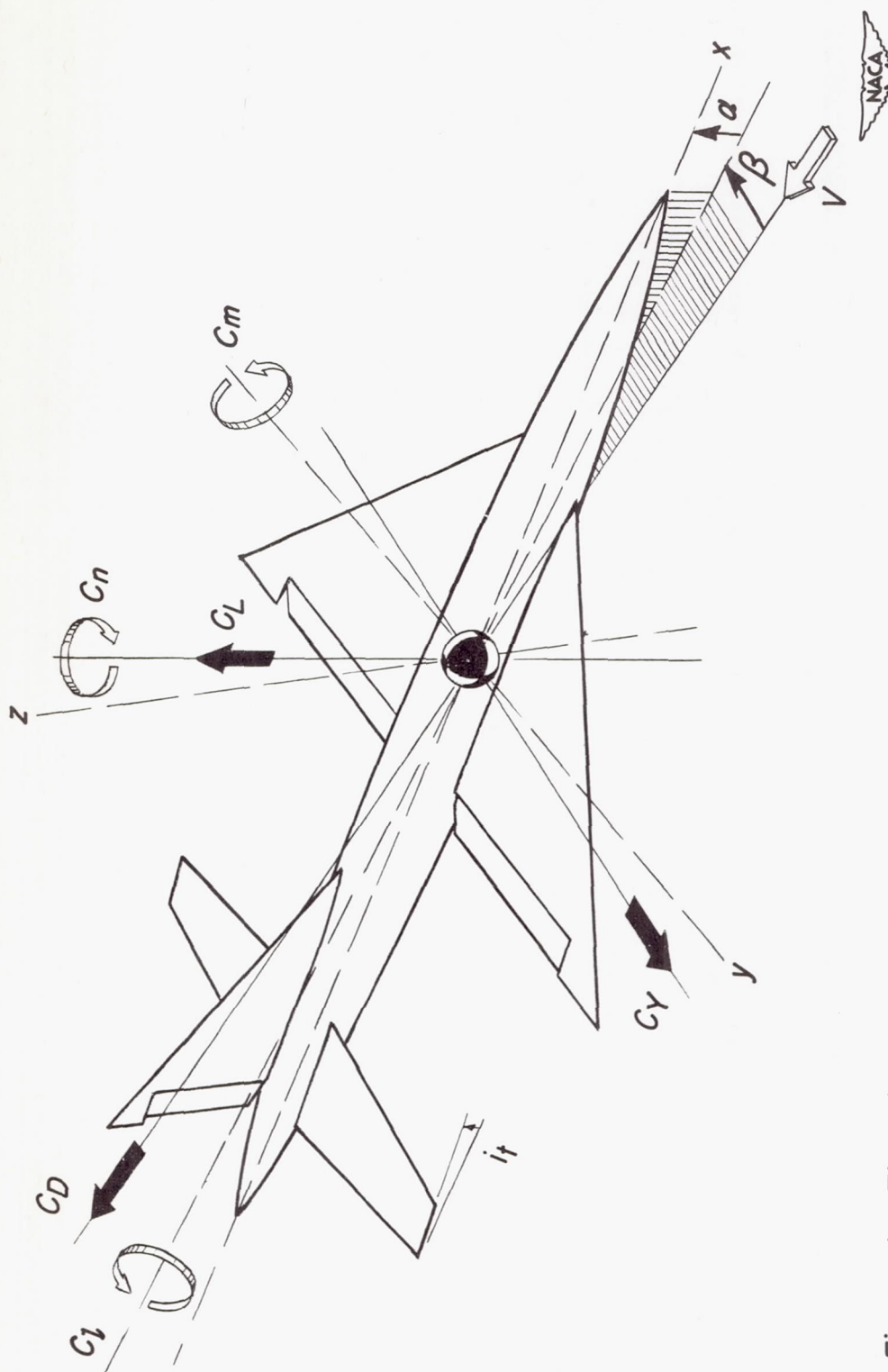
Figure 1.— The sign convention used in presentation of the data. All force and moment coefficients, angles, and control-surface deflections are shown as positive.

15.32

$\bar{c} = 13.65$

53.20°

$\dfrac{\bar{c}}{4}$

5.11

11.78

10.24

20.48

22.51

23.70

Pivot line

27.64

17.92

1.76

8.96

6.33

3.17

63.43°

Moment center location

Tail position	x
Low	2.54
Middle	2.61
High	3.21

x

56.16

Intersection of pivot line
and plane of symmetry
for the three horizontal
tail positions

Dimensions shown in feet
unless otherwise noted
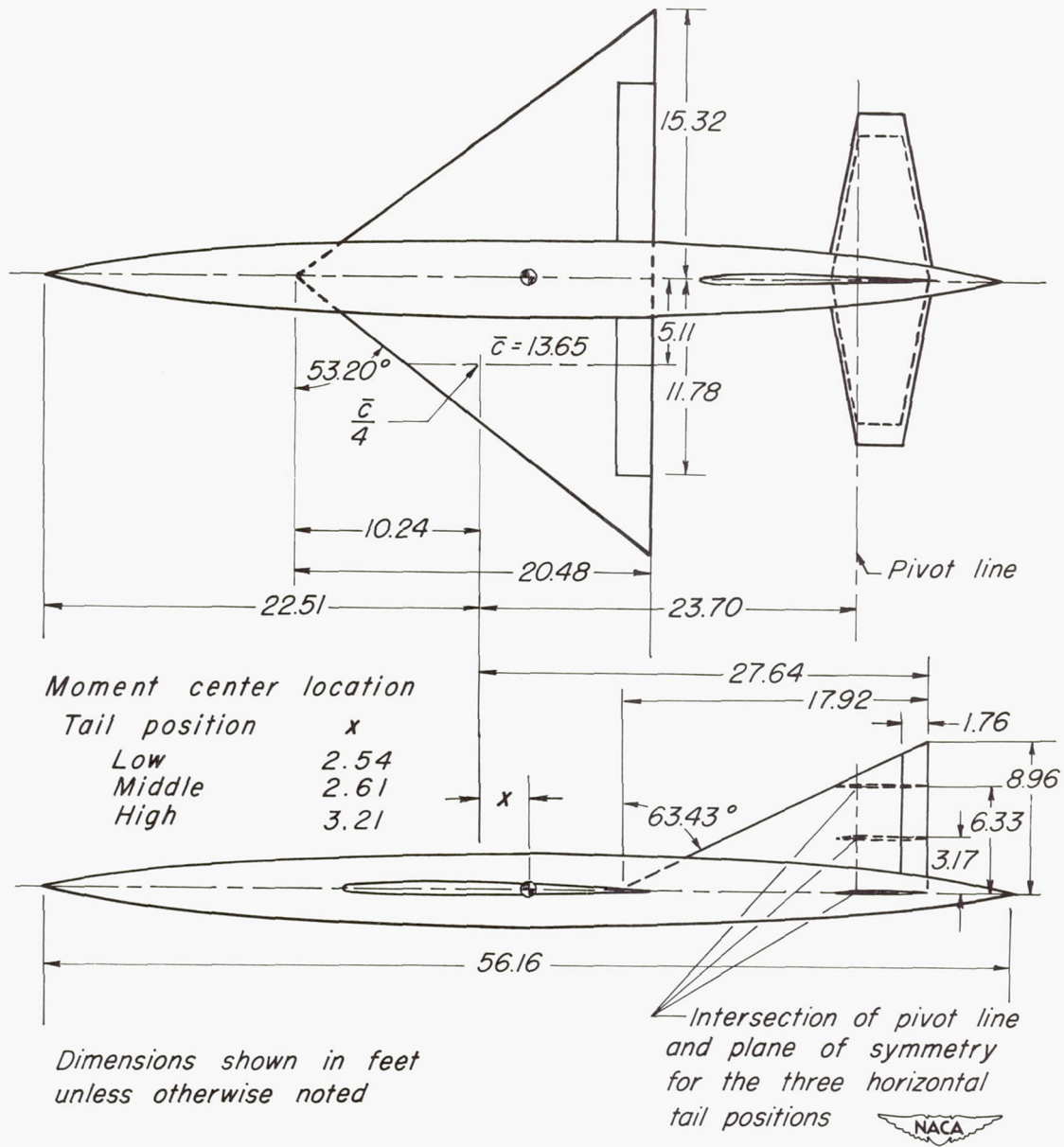
Figure 2.— Geometric details of the model.
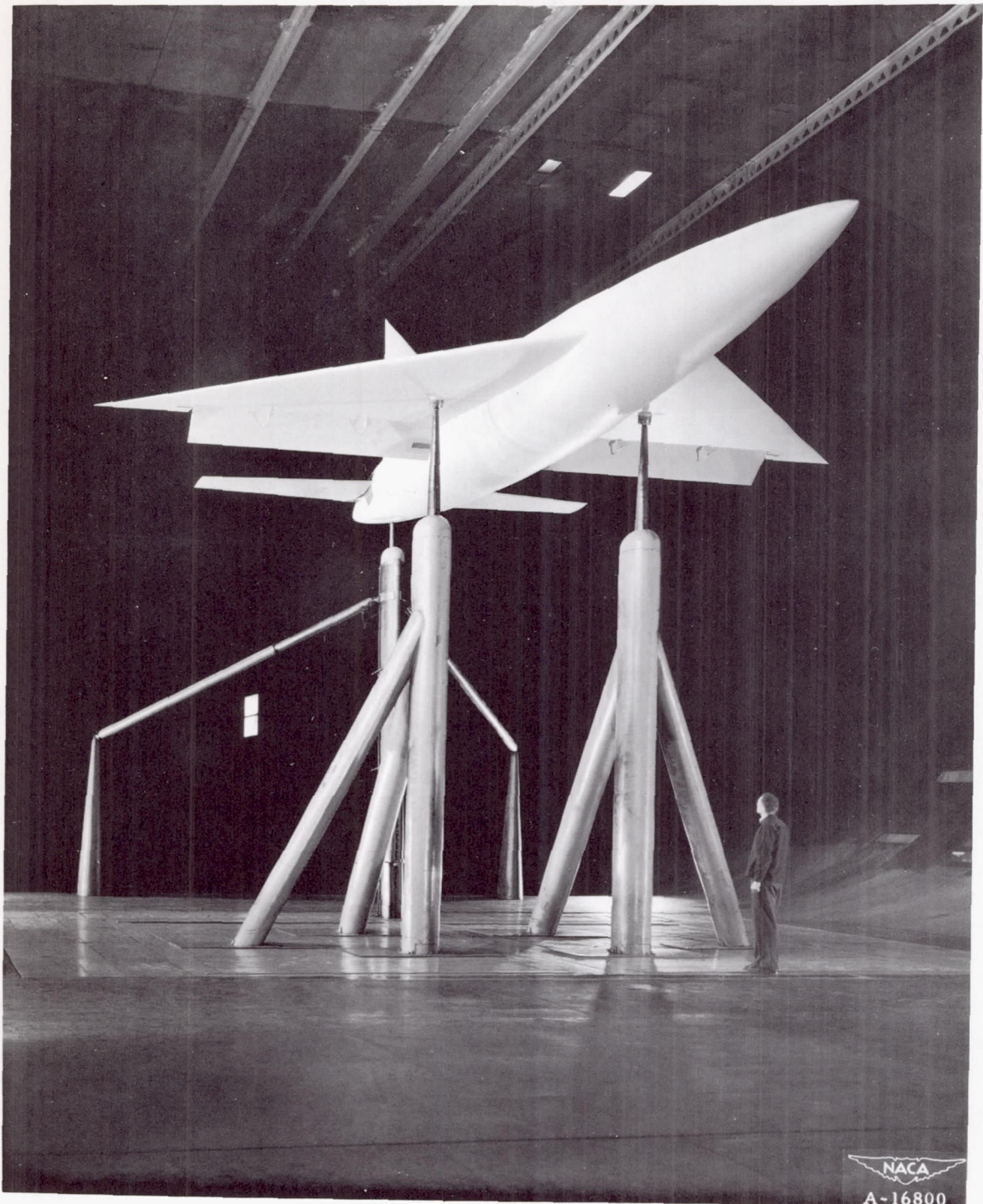
Figure 3.- The model with trailing-edge flaps deflected mounted in the
Ames 40- by 80-foot wind tunnel.

Model center line

Area of plan form with
section arbitrarily faired
with a maximum of 0.1−
percent−chord deviation.

Note: All dimensions
are in feet.

4.12

9.10

6.66

7.32

Contour of fuselage at
wing chord plane
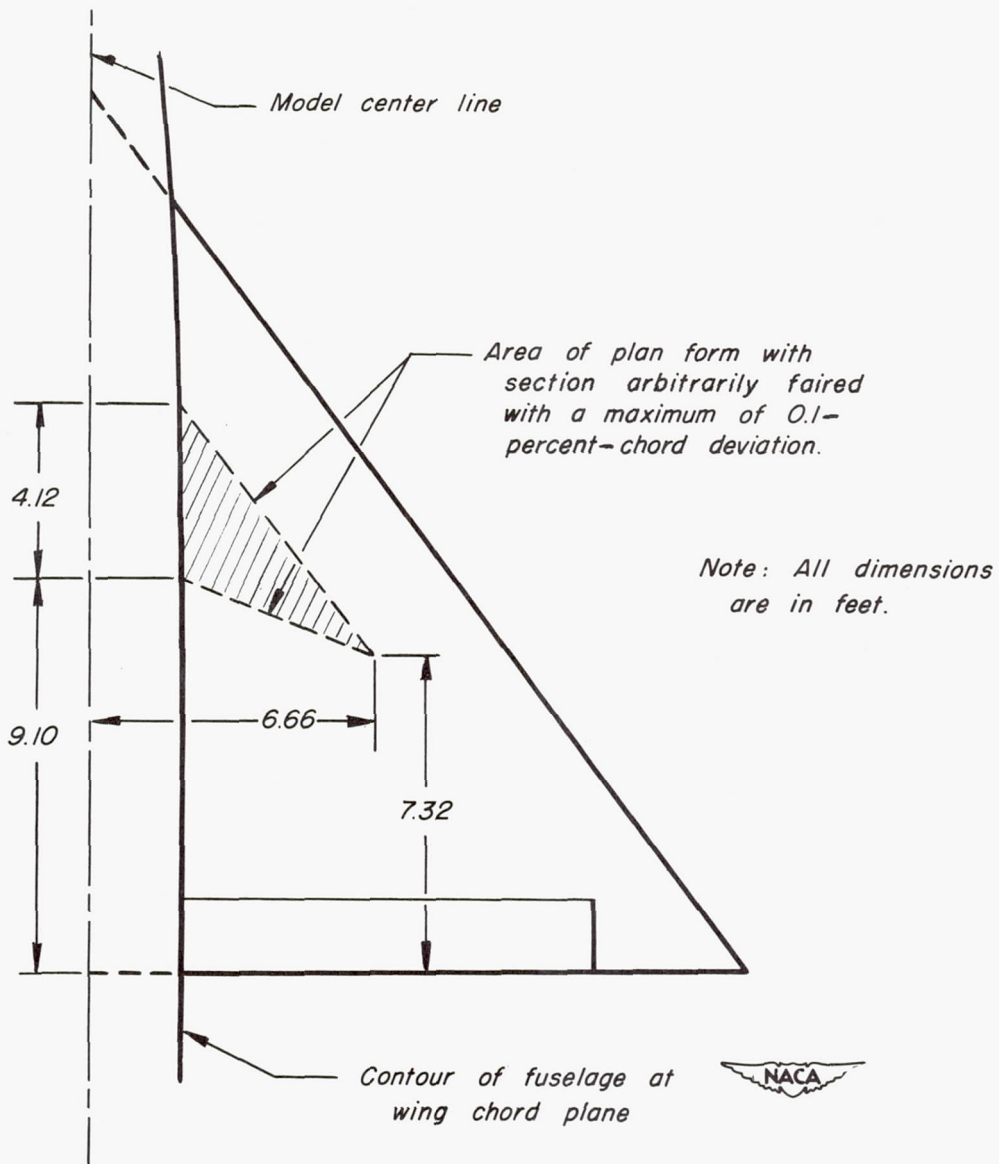
NACA

Figure 4.— The area on each wing panel of the model where
the wing section deviates slightly from the NACA 0005
(modified) section.

Section of flap nose shown
parallel to model center line
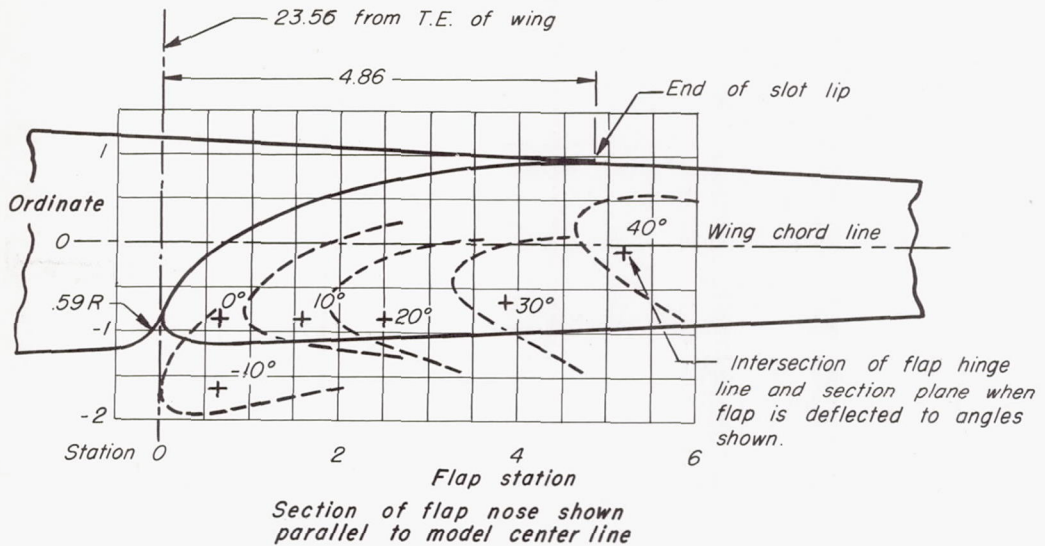
Flap coordinates for all spanwise station		
Station	Upper Surface	Lower Surface
0	- 0.872	- 0.872
0.113	- .554	- 1.030
.226	- .408	- 1.086
.452	- .181	- 1.119
.679	- .012	- 1.131
1.357	.351	- 1.119
2.036	.589	- 1.086
2.714	.747	- 1.041
3.393	.860	- 1.006
4.071	.905	- 0.973
4.750	.916	- 0.938
5.654	.905	- 0.905
11.309	.610	- 0.610
16.963	.328	- 0.328
23.560	0	0
Center of L.E. arc		
0.17	-0.87	
L.E. radius: 0.17		

Dimensions shown
in inches

Figure 5.— Geometric data of the flap and slot profile used on the
trailing-edge, constant-chord, slotted flaps.
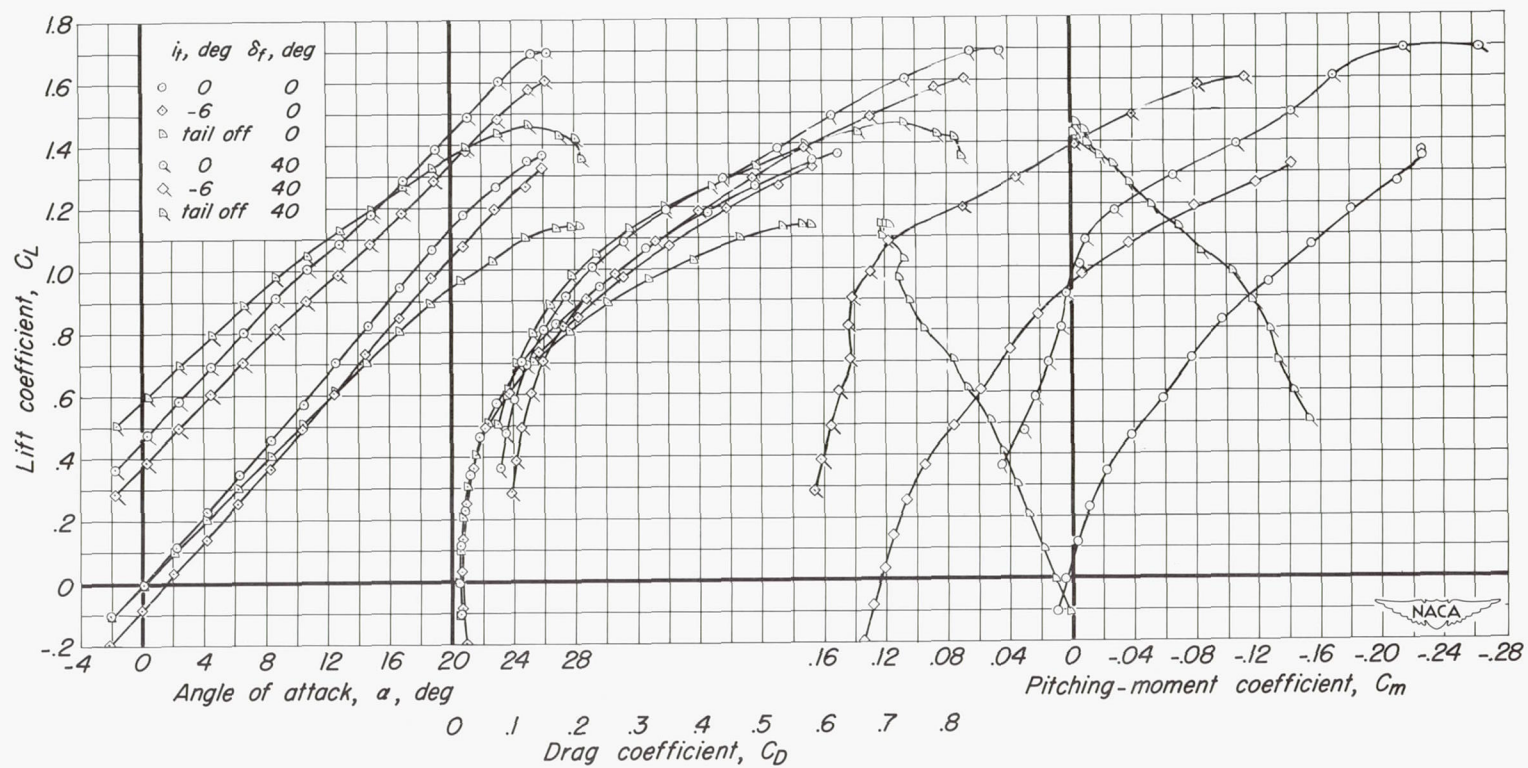
Figure 6.– Longitudinal characteristics of the model with the horizontal tail in the low position. $\frac{z}{b/2}$, O; moment center, 0.436$\bar{c}$.
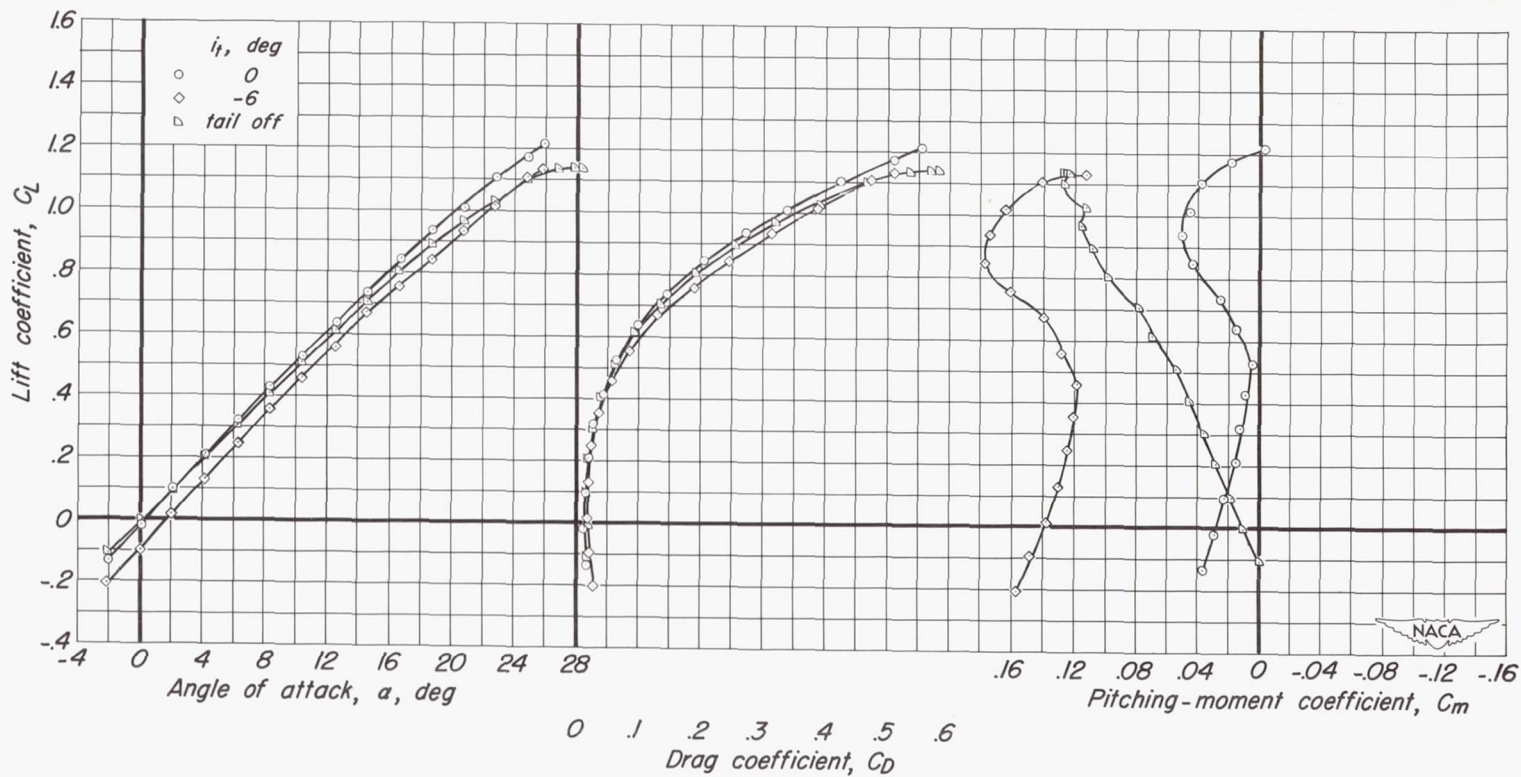
Figure 7.– Longitudinal characteristics of the model with the horizontal tail in the middle position. $\frac{z}{b/2}$, 0.21; moment center, 0.441$\bar{c}$; δ_f, 0°.
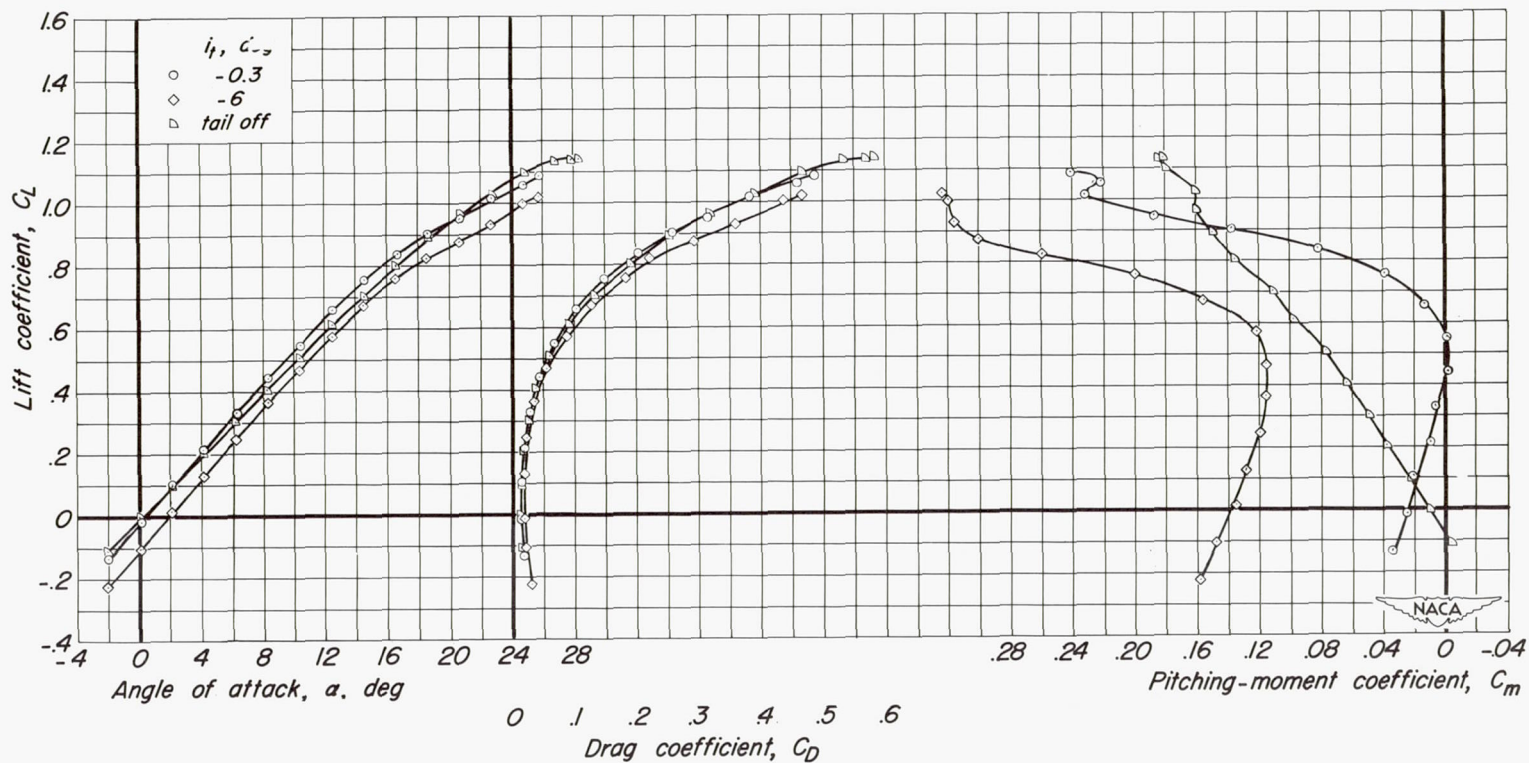
Figure 8.- Longitudinal characteristics of the model with the horizontal tail in the high position. $\frac{z}{b/2}$, 0.41; moment center, 0.485 $\bar{c}$; δ_f, 0°
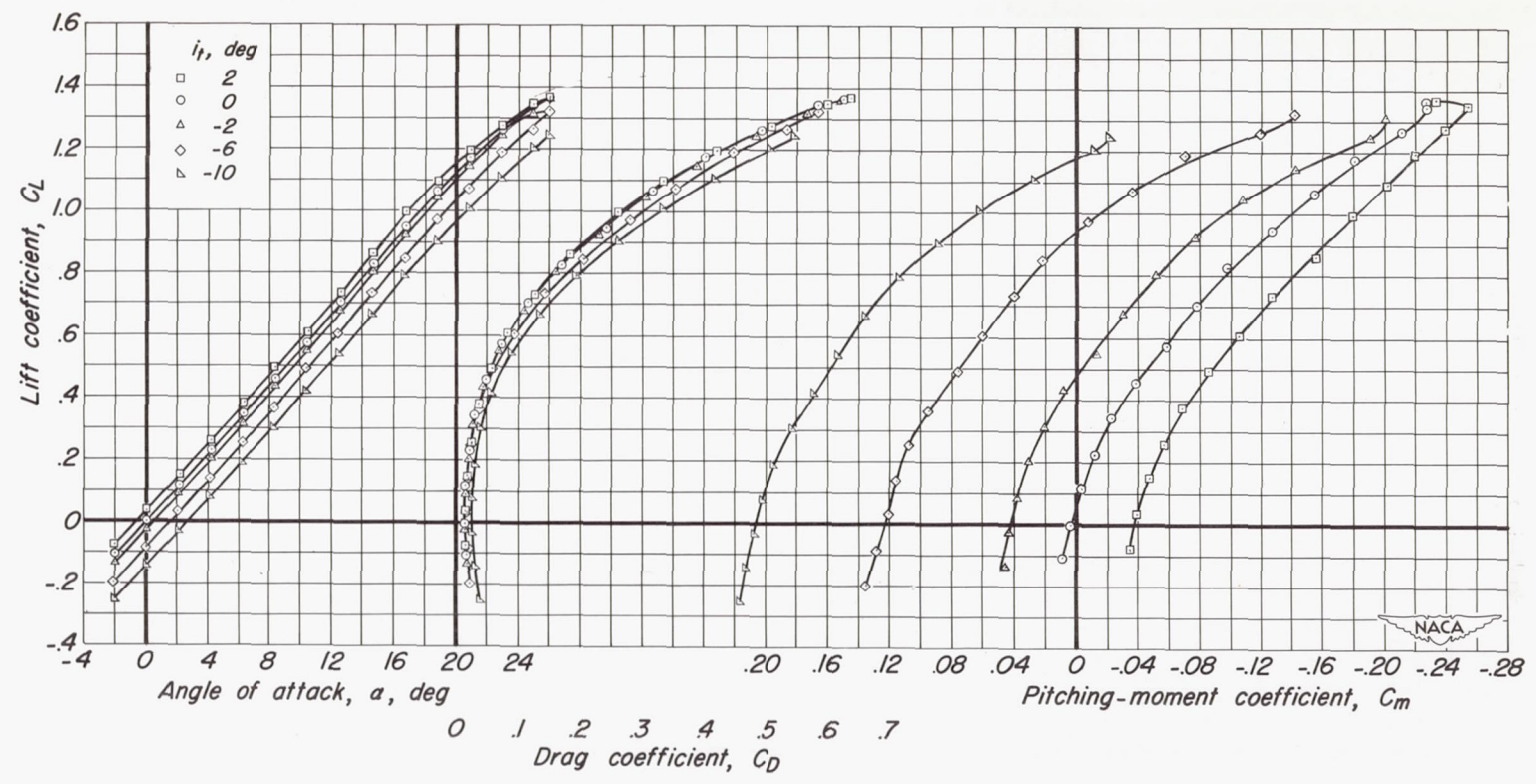
(a) δ_f, $0°$

Figure 9.— The effect of the horizontal tail in the low position on the longitudinal characteristics of the model for two flap deflections. $\frac{z}{b/2}$, 0; moment center, $0.436\bar{c}$.
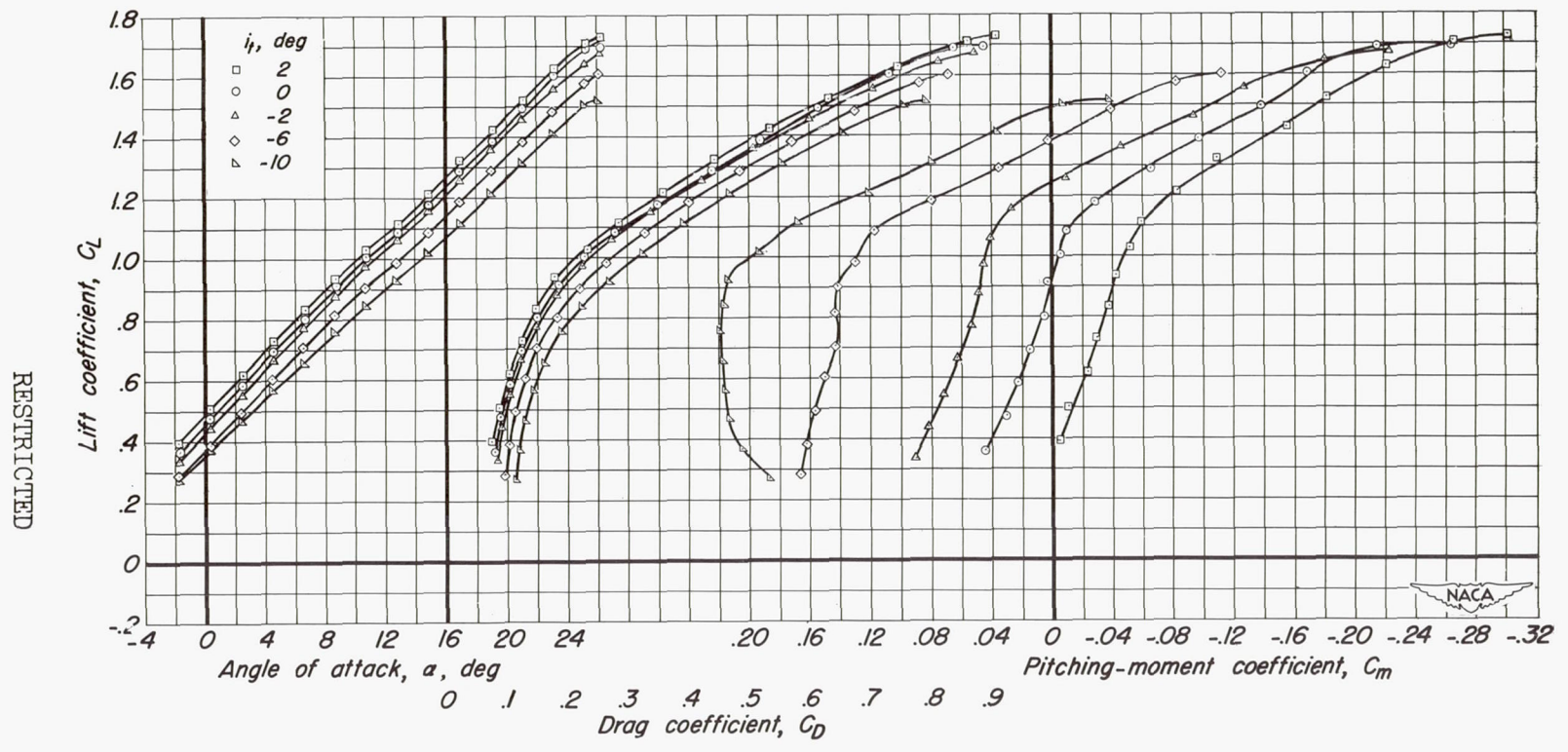
(b) δ_f , 40°

Figure 9.— Concluded.

β, deg	δf, deg
○ 0	0
□ 6	0
△ 12	0
0	40
6	40
12	40
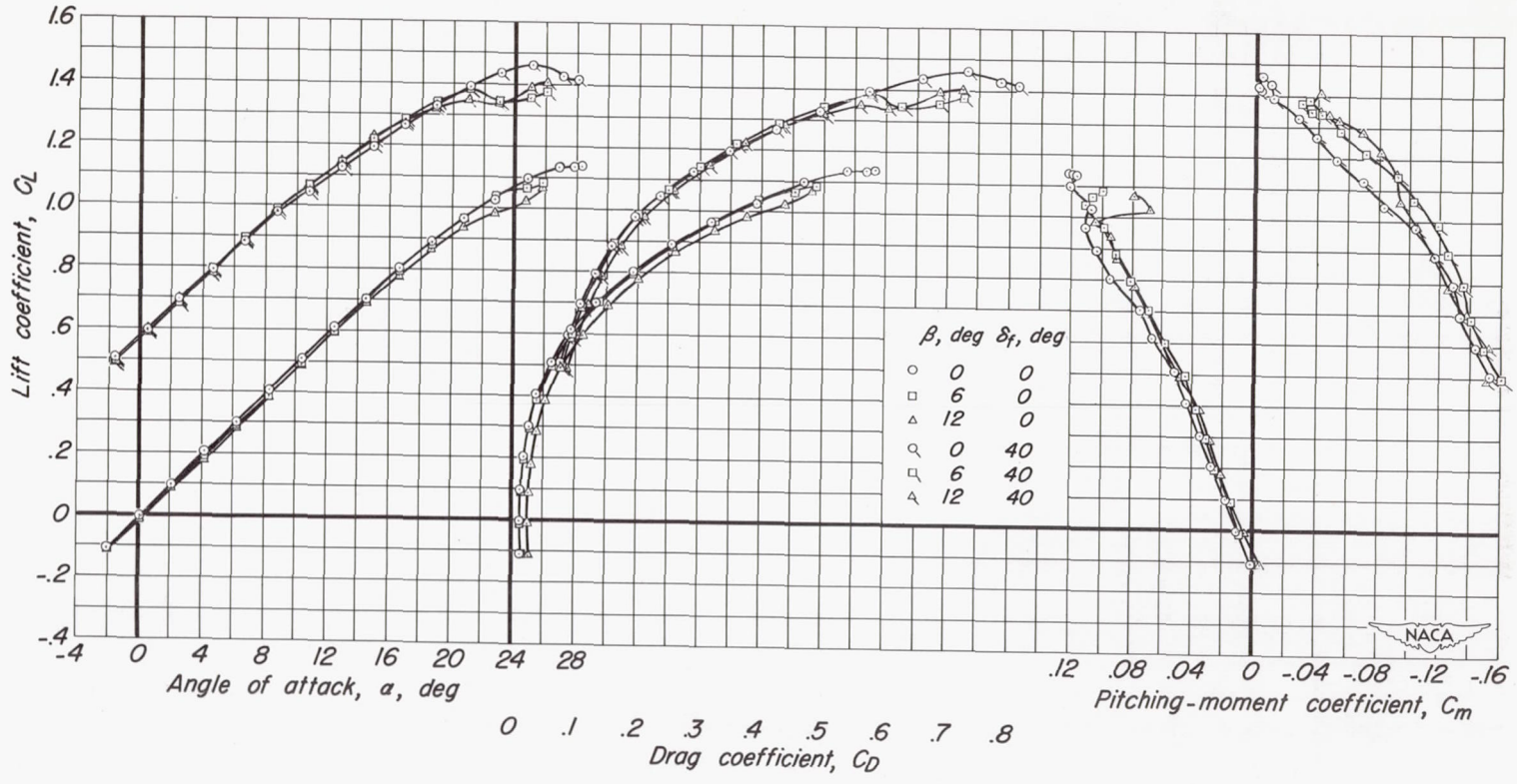
(a) C_L vs $α$, C_D, C_m

Figure 10.— Characteristics of the model without the horizontal tail at three angles of sideslip;
Moment center, $0.436\bar{c}$.
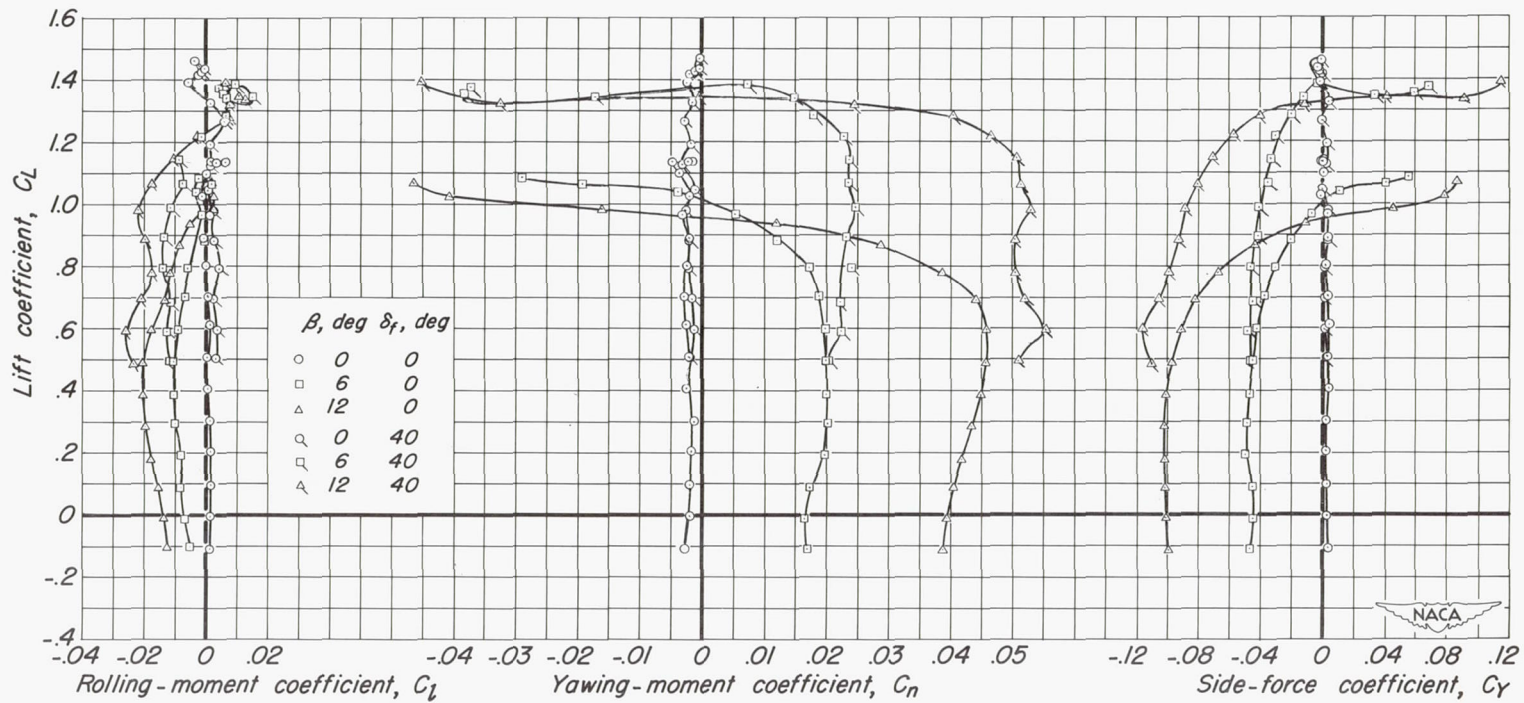
(b) C_L vs C_l, C_n, C_Y

Figure 10.— Concluded.
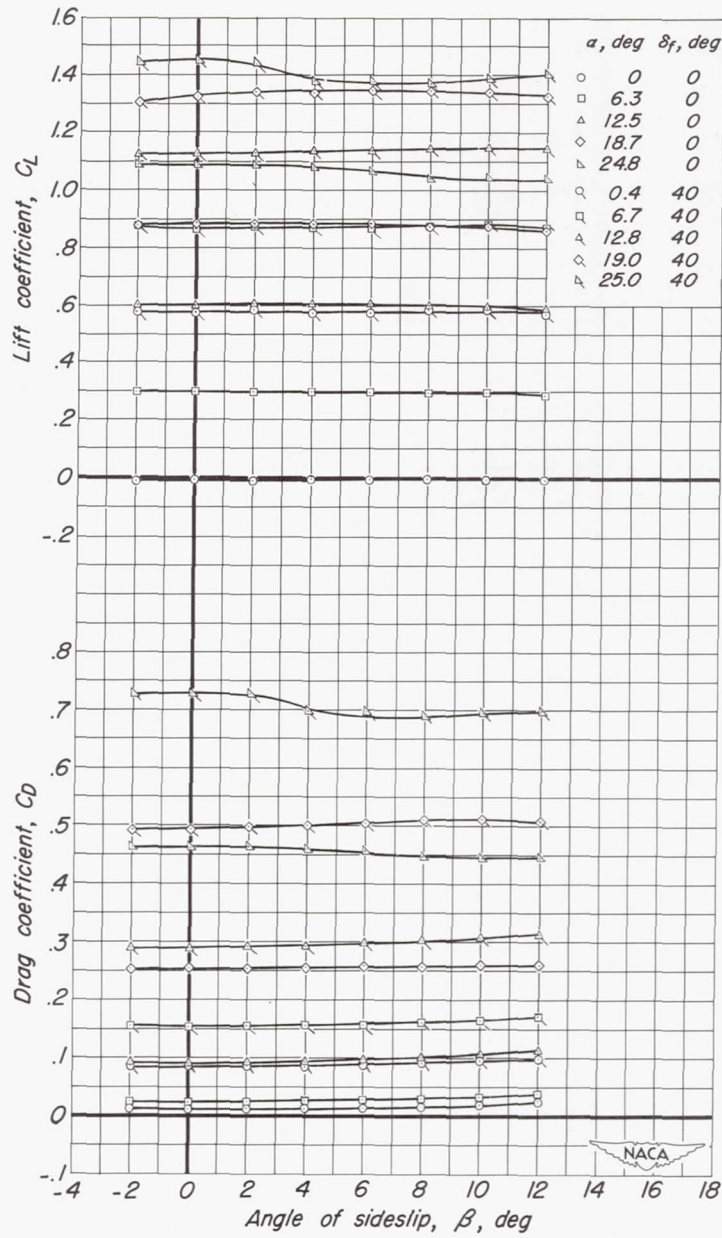
(a) C_L, C_D vs β

Figure 11.— Characteristics of the model in
sideslip without the horizontal tail.
Moment center, $0.436\bar{c}$.

a, deg	δ_f, deg
0	0
6.3	0
12.5	0
18.7	0
24.8	0
0.4	40
6.7	40
12.8	40
19.0	40
25.0	40
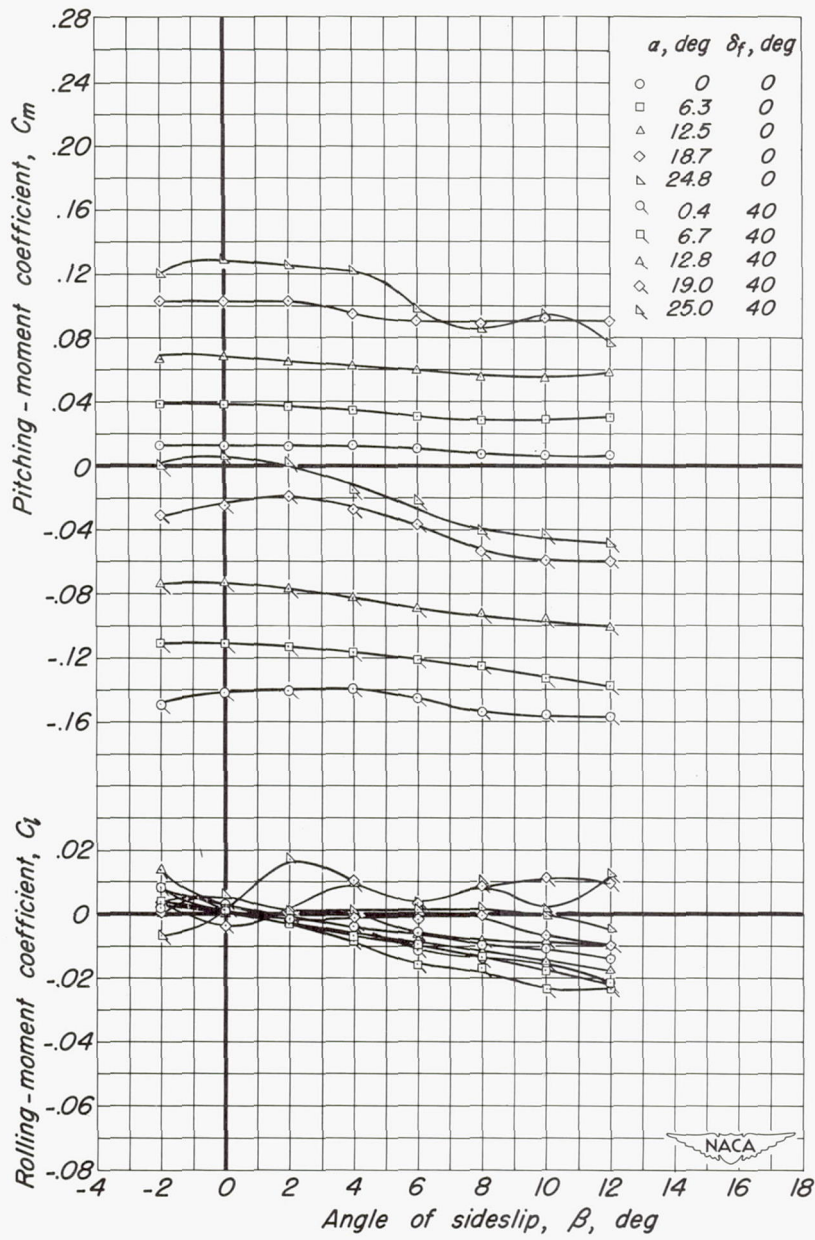
(b) C_m, C_l vs β

Figure 11.— Continued.
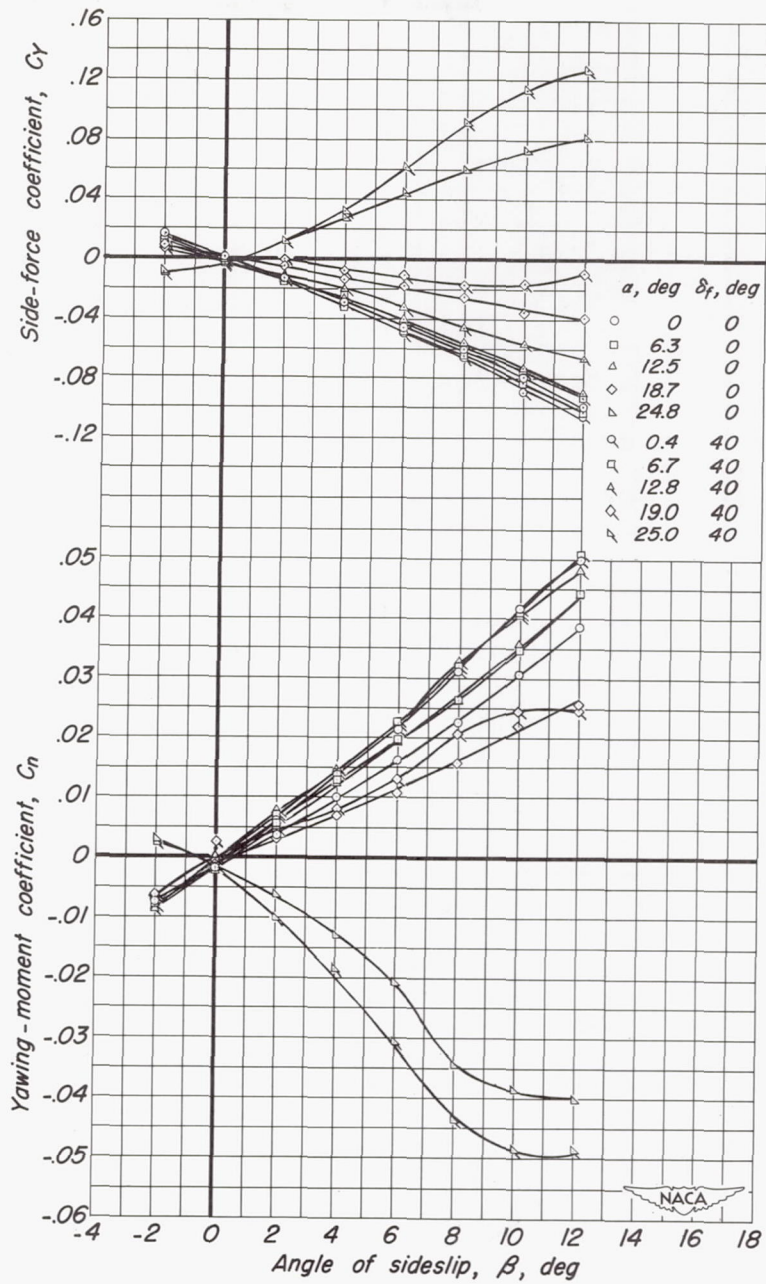
(c) C_Y, C_n vs β

Figure 11.- Concluded.
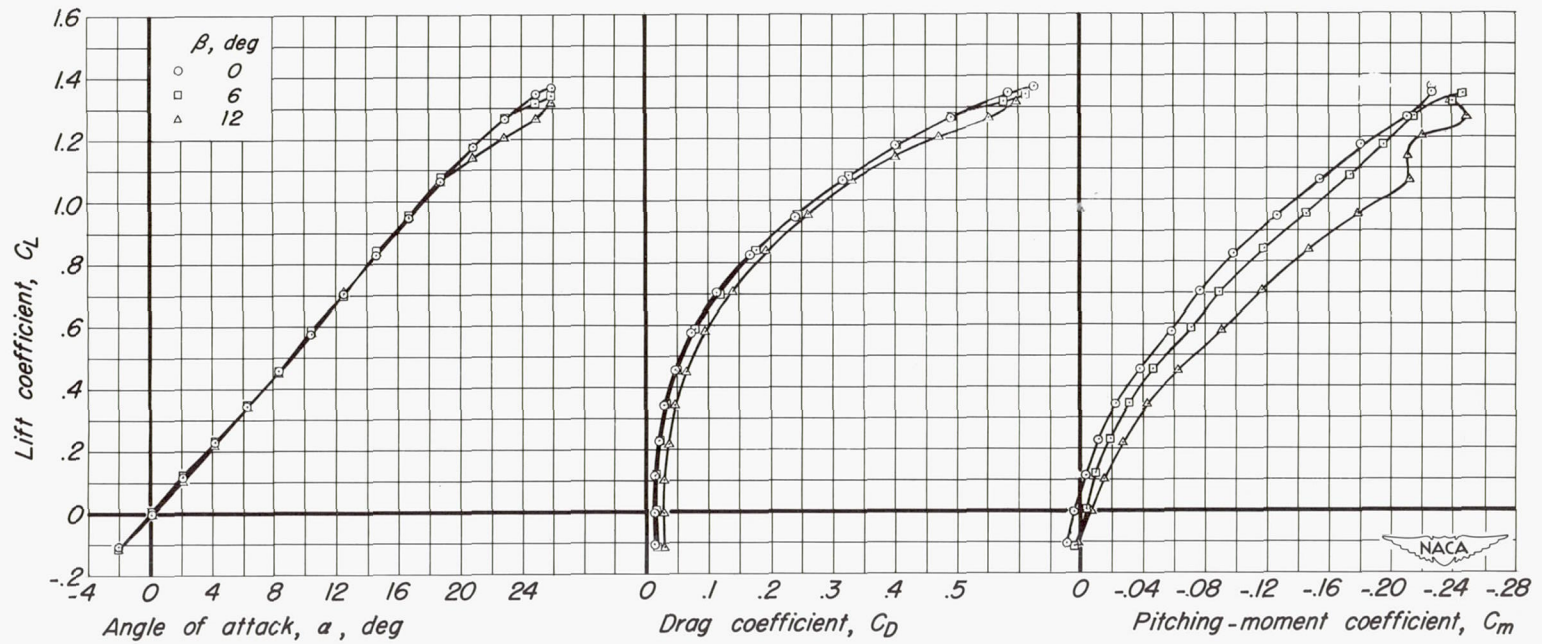
(a) C_L vs α, C_D, C_m

Figure 12.— Characteristics of the complete model at three angles of sideslip. $\frac{z}{b/2}$, 0; moment center $0.436\bar{c}$; i_t, $0°$; δ_f, $0°$.
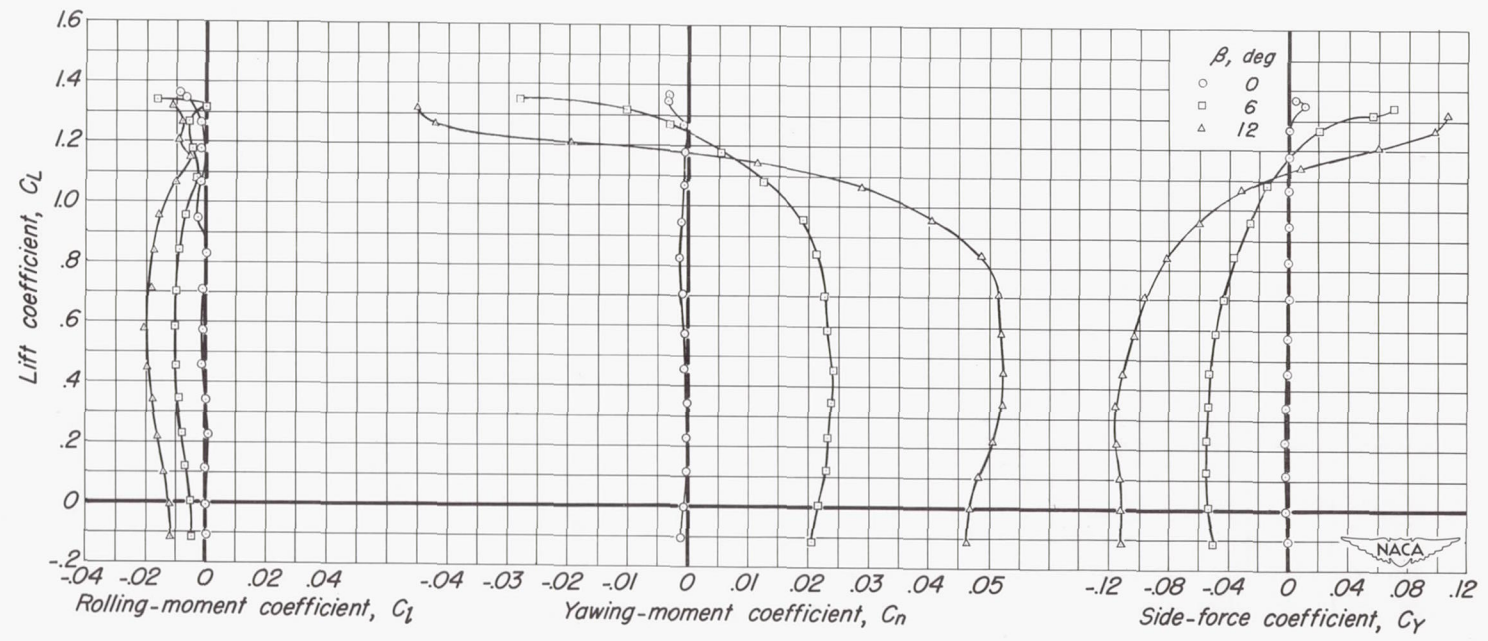
(b) C_L vs C_l, C_n, C_Y

Figure 12.— Concluded.
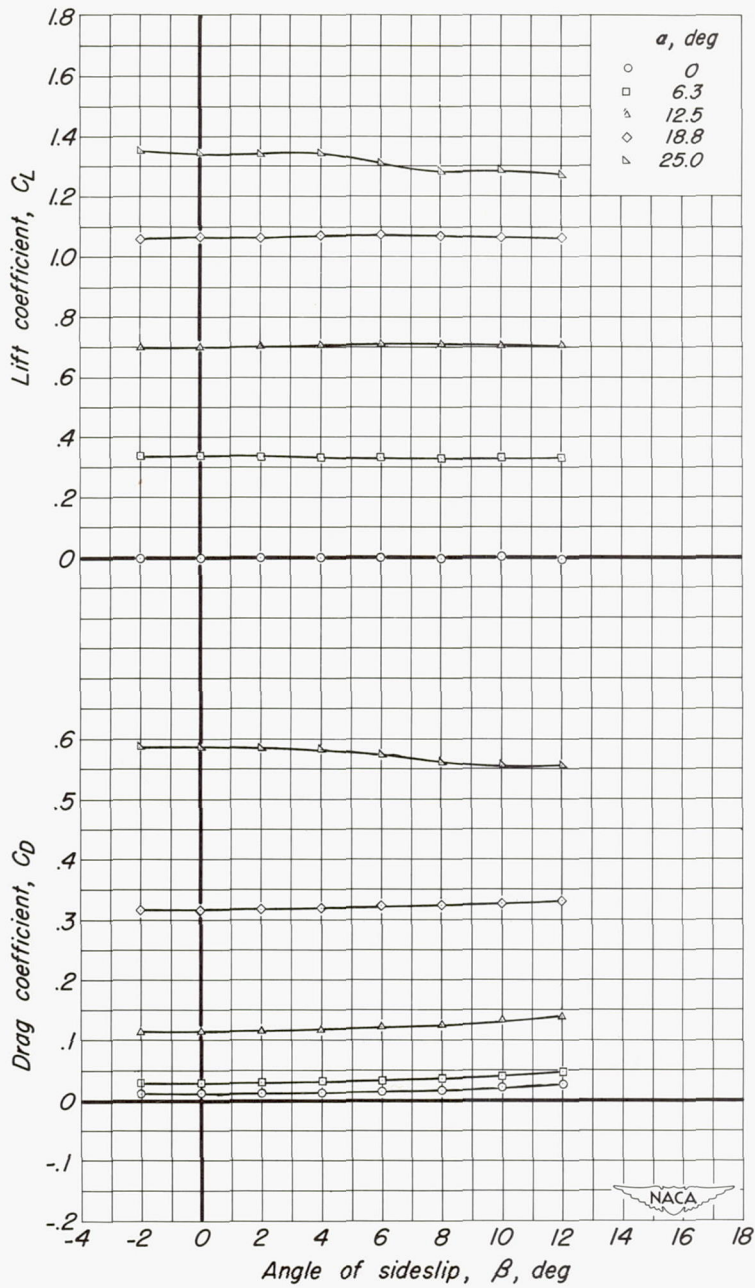
(a) C_L , C_D vs β

Figure 13.- Characteristics of the complete model in sideslip. $\frac{z}{b/2}$, 0; moment center, 0.436$\bar{c}$; i_t, 0°; δ_f, 0°.
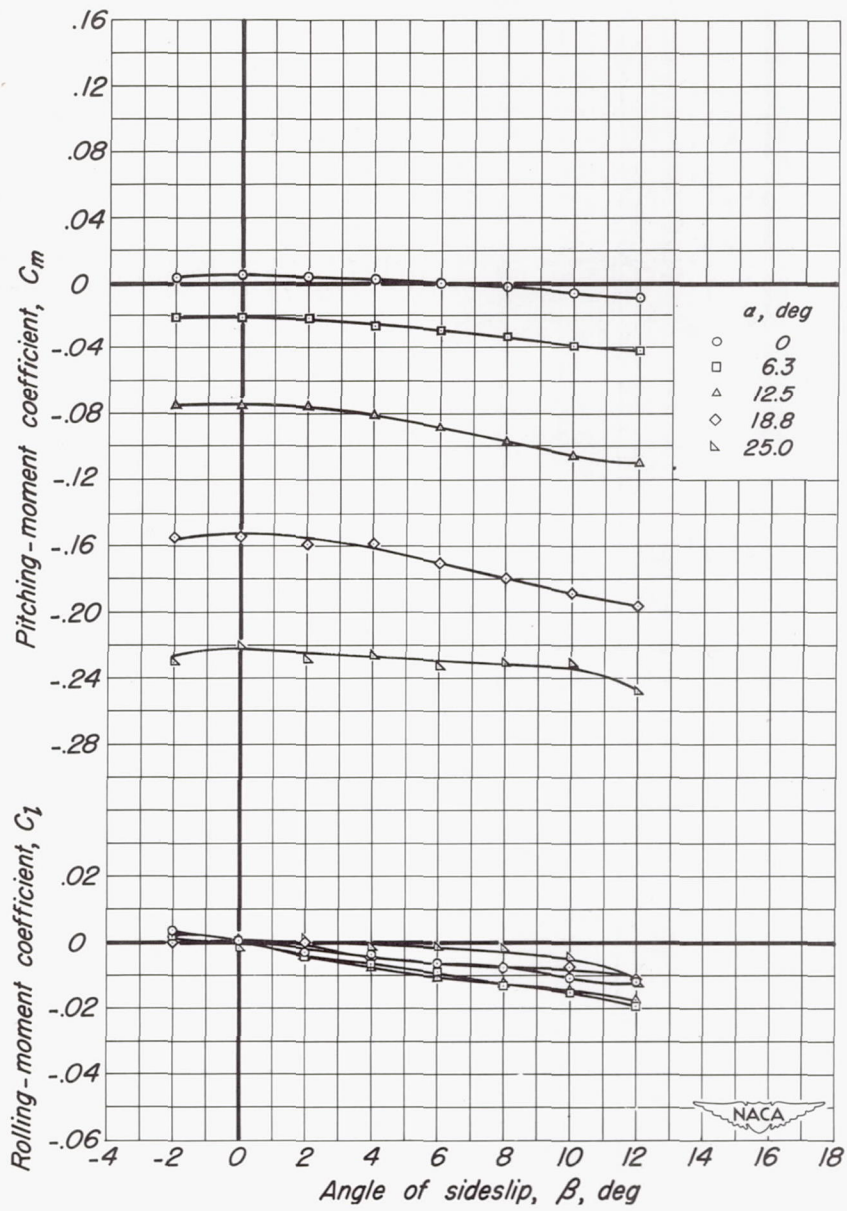
(b) C_m, C_l vs β

Figure 13.- Continued.
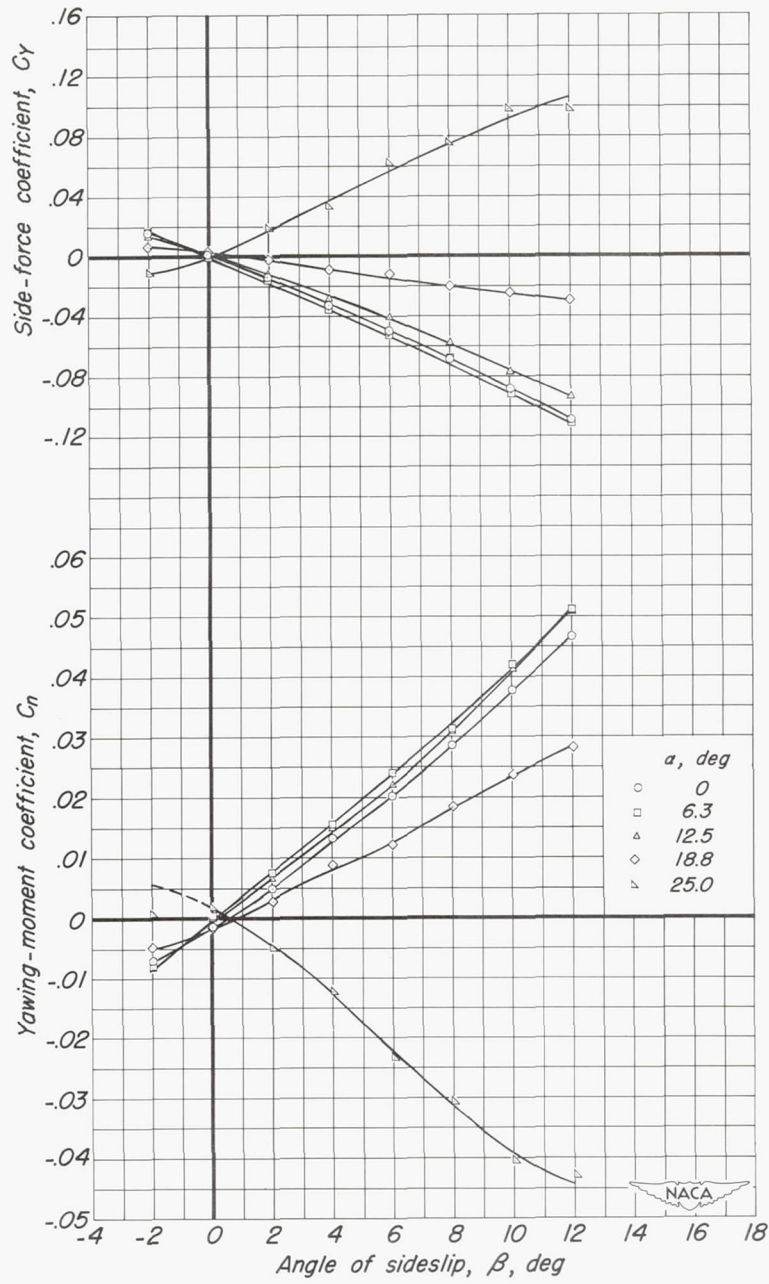
(c) C_Y, C_n vs β

Figure 13.— Concluded.
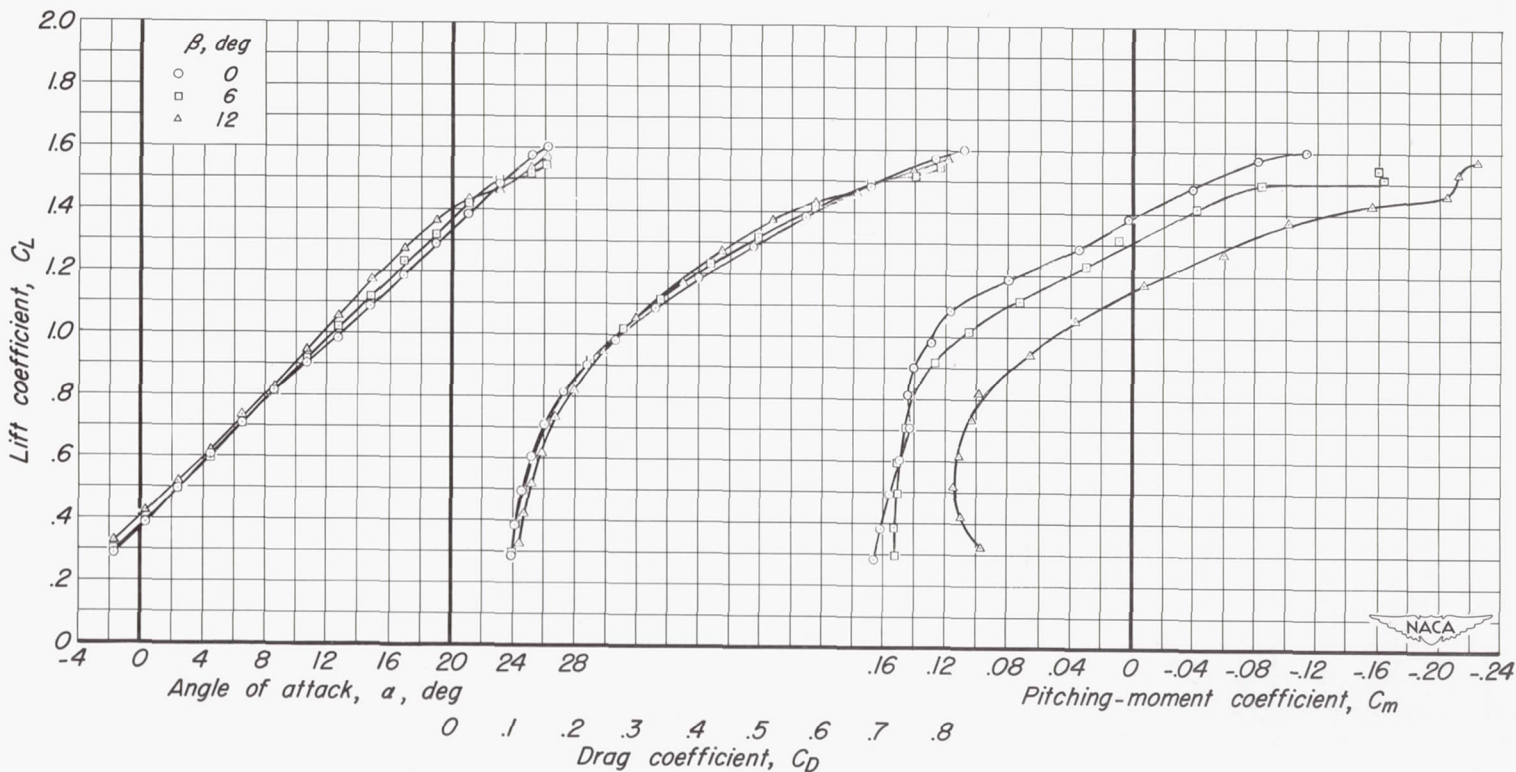
(a) C_L vs a, C_D, C_m

Figure 14.- Characteristics of the complete model at three angles of sideslip. $\frac{z}{b/2}$, 0; moment center, 0.436; i_t, -6°; δ_f, 40°.
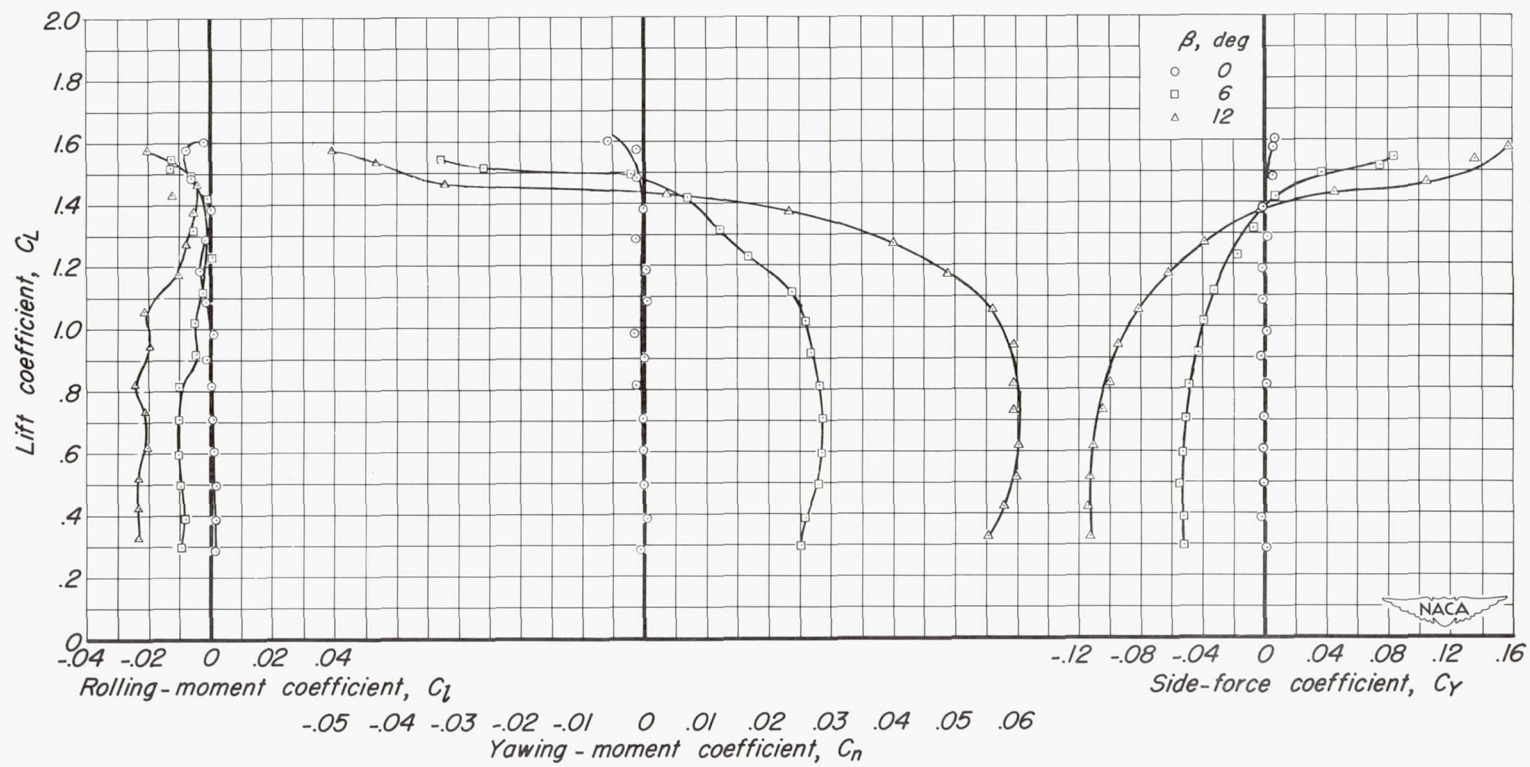
(b) C_L vs C_l , C_n , C_Y

Figure 14.- Concluded.
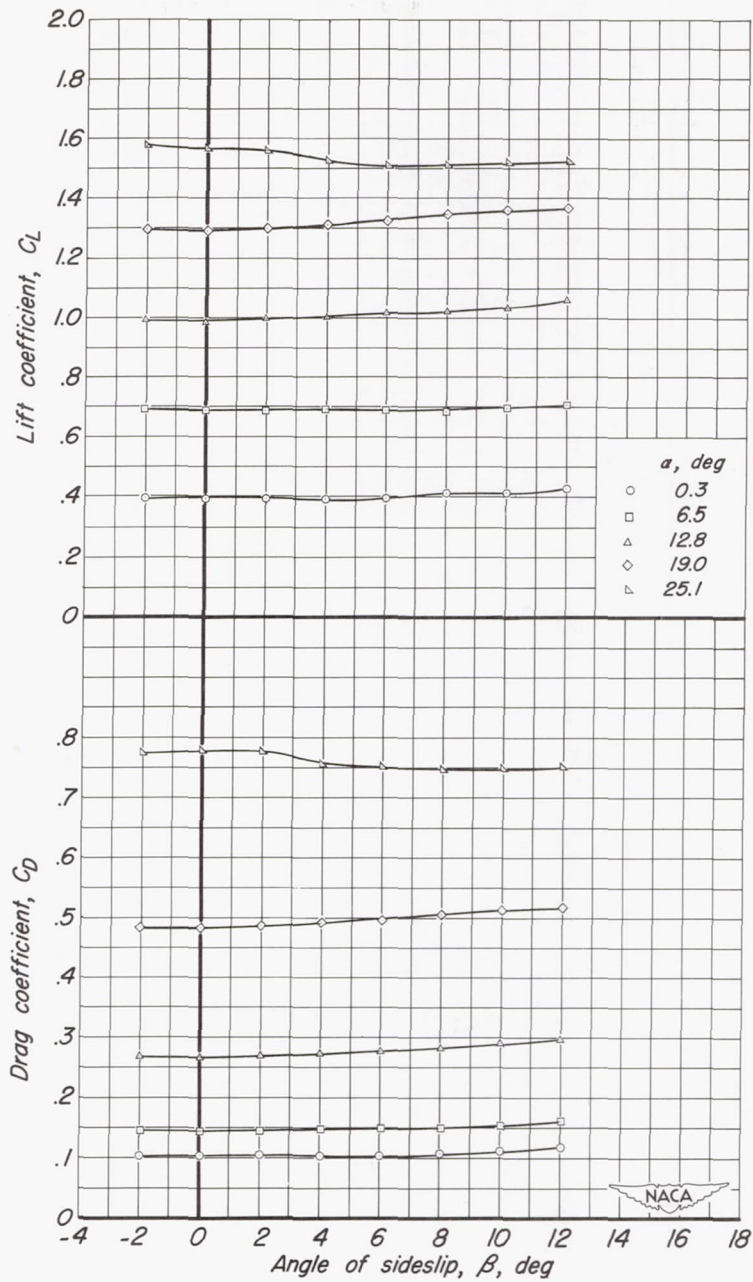
(a) C_L, C_D vs β

Figure 15.— Characteristics of the complete model in sideslip. $\frac{z}{b/2}$, 0; moment center $0.436\bar{c}$; i_t, -6°; δ_f, 40°.
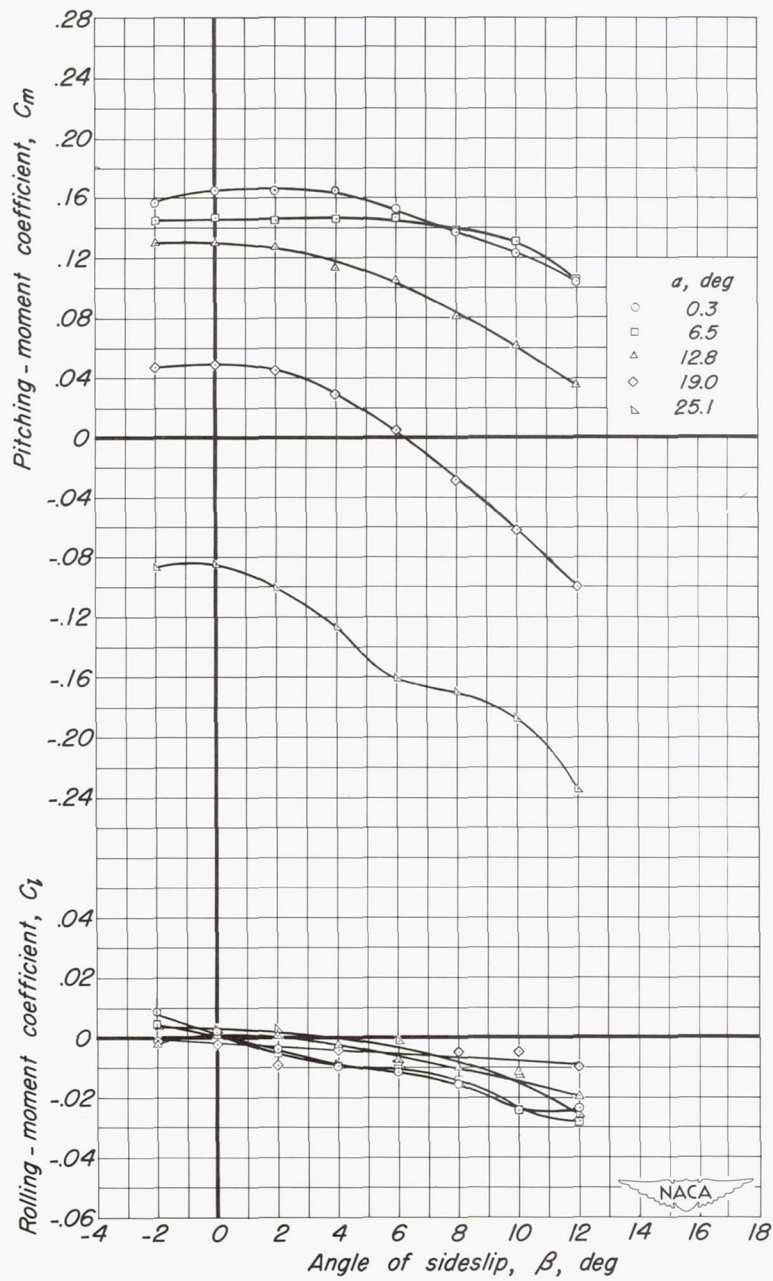
(b) C_m, C_l vs β

Figure 15.- Continued.
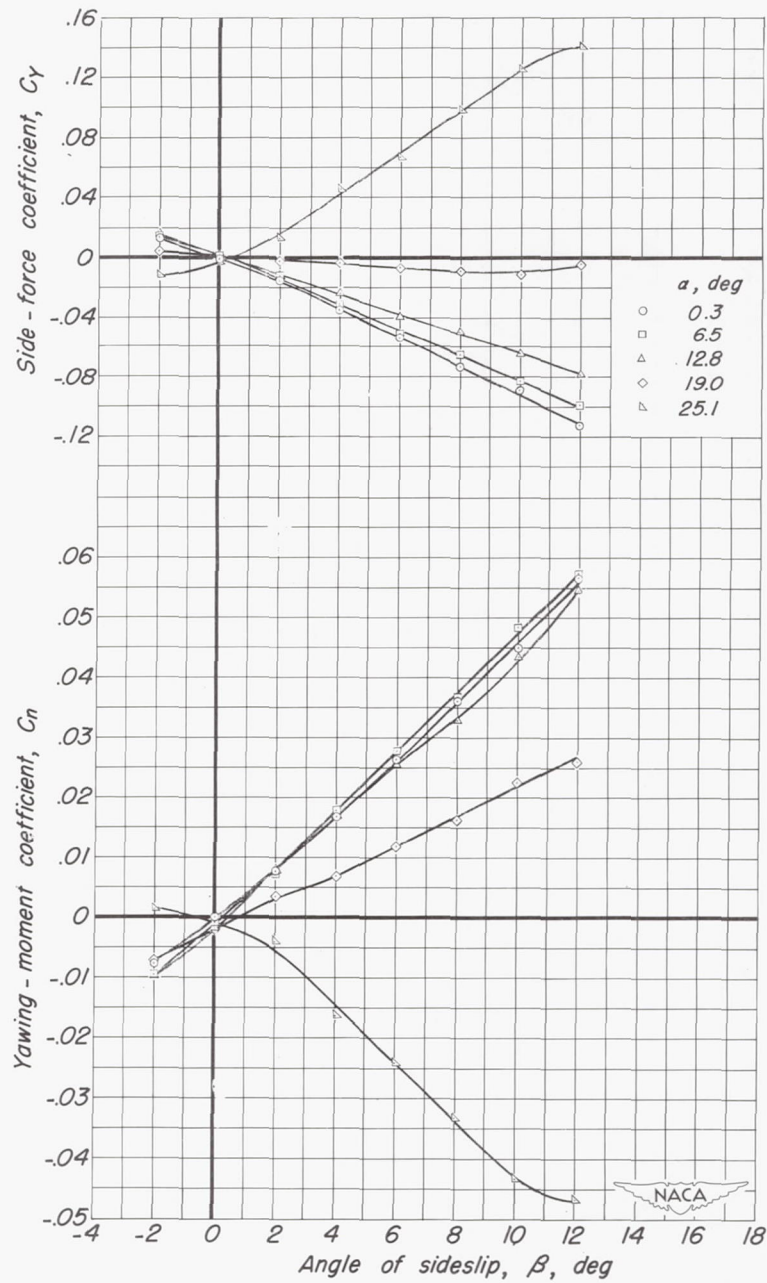
(c) C_Y, C_n vs β

Figure 15.- Concluded.
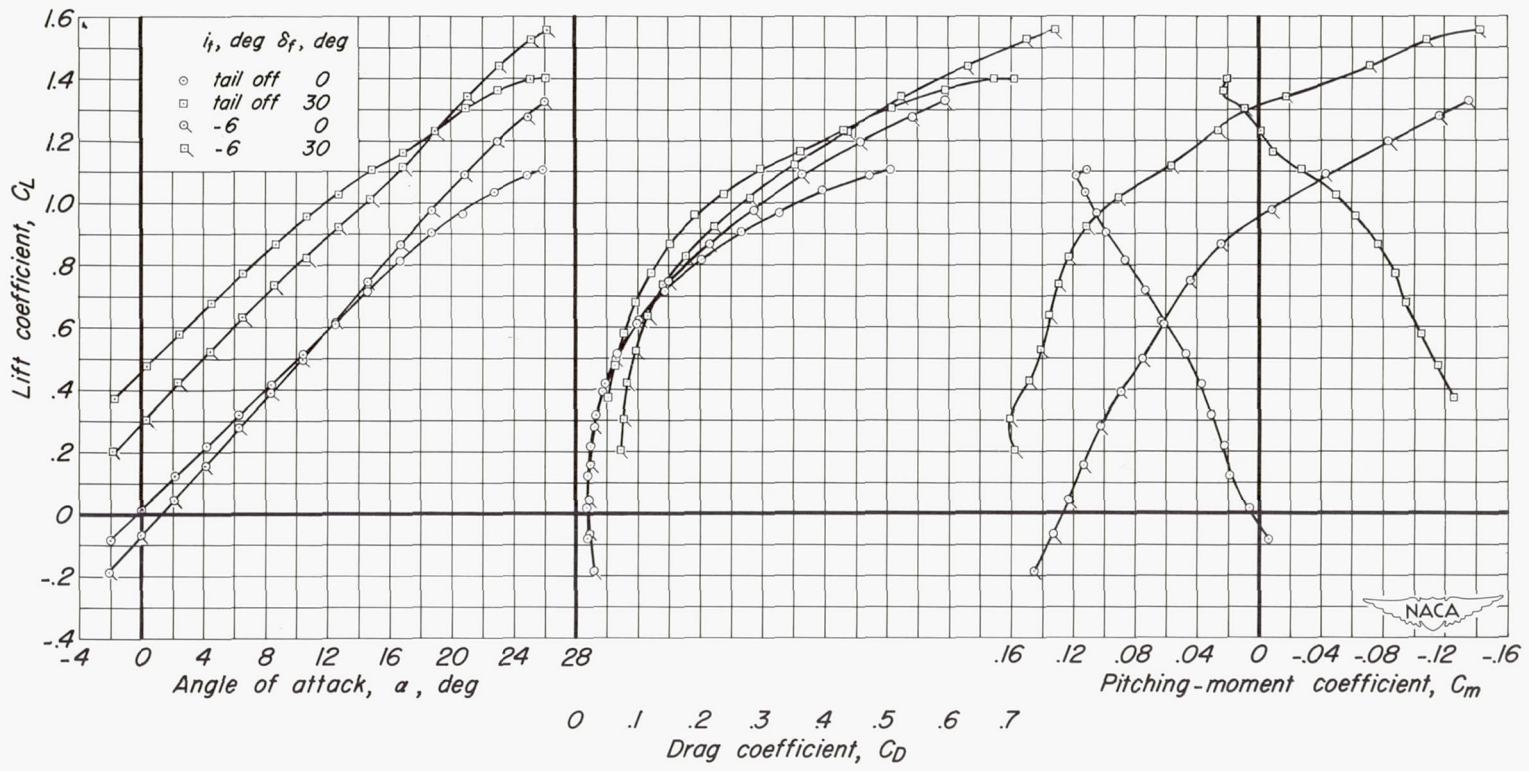
(a) C_L vs α, C_D, C_m

Figure 16.- The effect of the horizontal tail on the characteristics of the model at zero sideslip with flaps used as lateral-control devices. $\frac{z}{b/2}$, O; moment center, $0.436\bar{c}$; δ_{lf}, $20°$.

(b) C_L vs C_l , C_n , C_Y

Figure 16.- Concluded
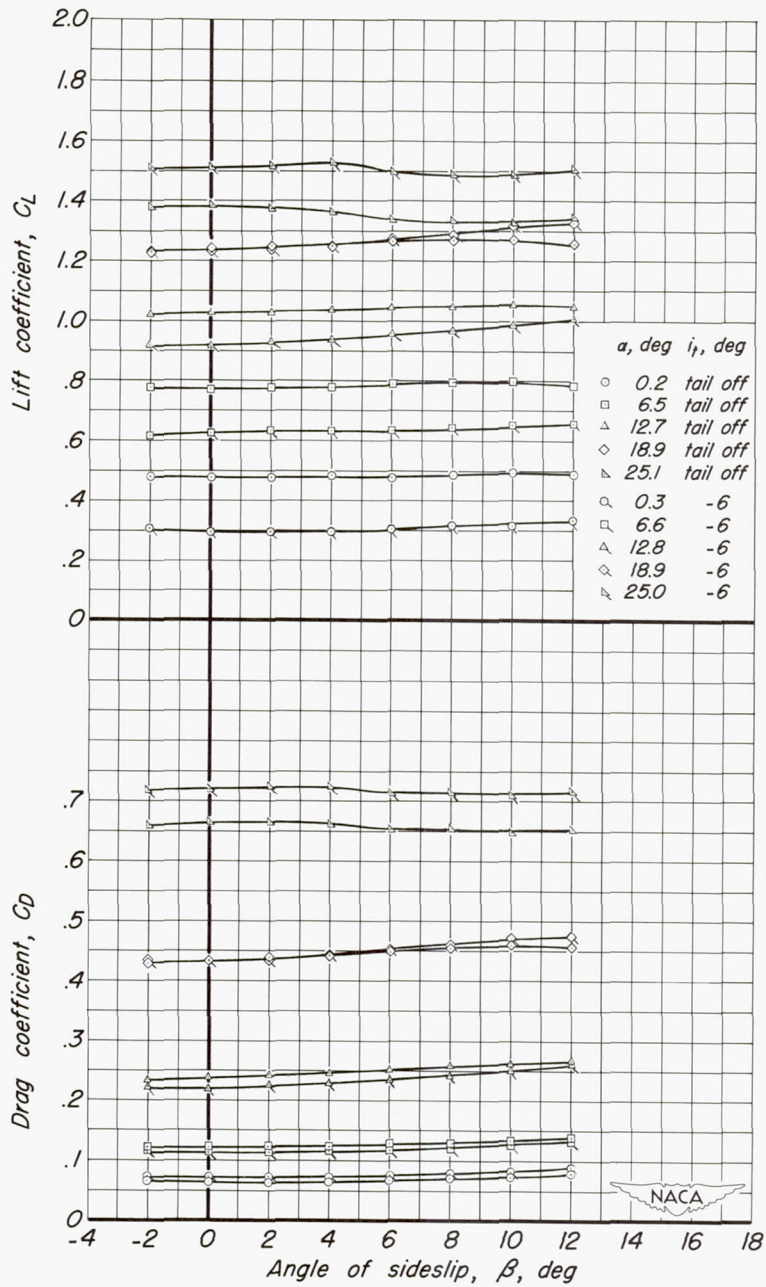
(a) C_L, C_D vs β

Figure 17.— The effect of the horizontal tail on the characteristics of the model in sideslip with the flaps used as lateral-control devices. $\frac{z}{b/2}$, 0; moment center 0.436$\bar{c}$; δ_{l_f}, 20°; δ_f, 30°.
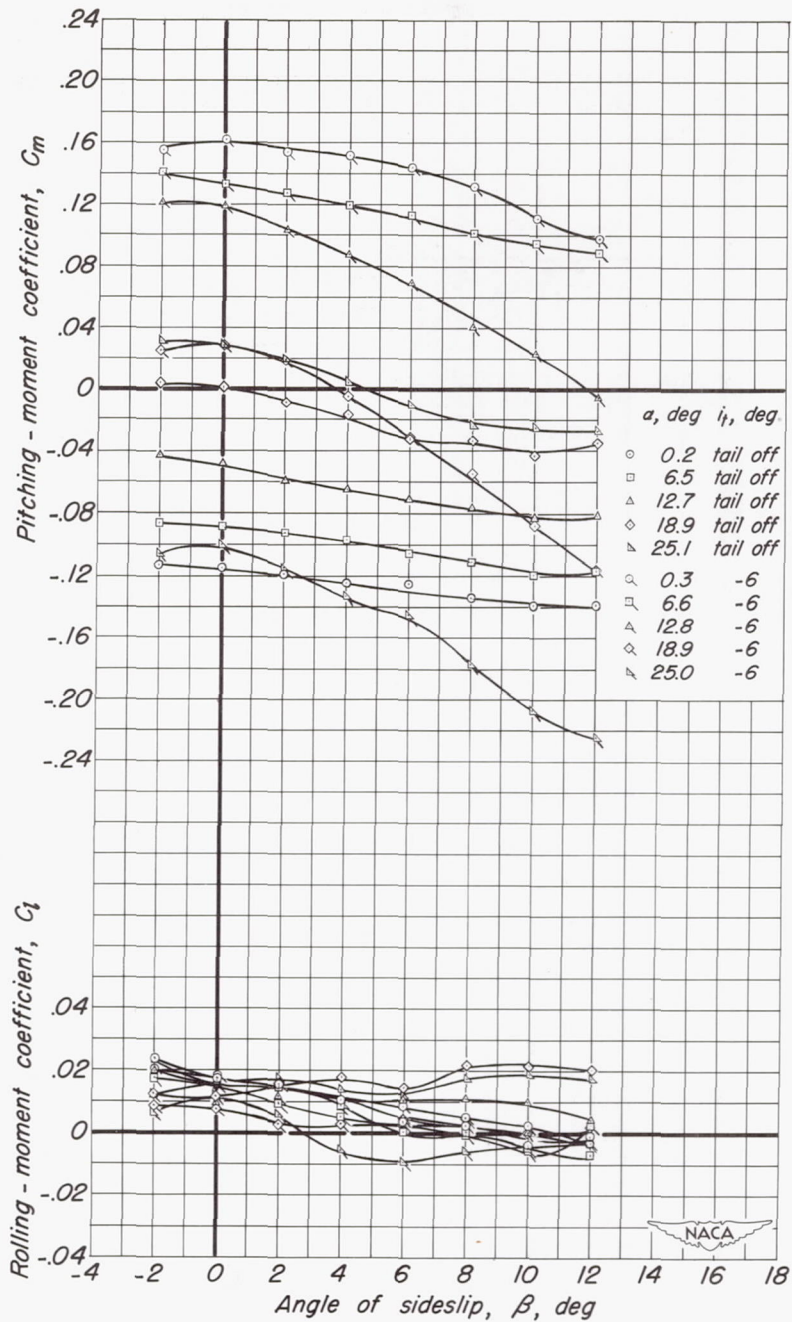
(b) C_m, C_l vs β

Figure 17.— Continued.
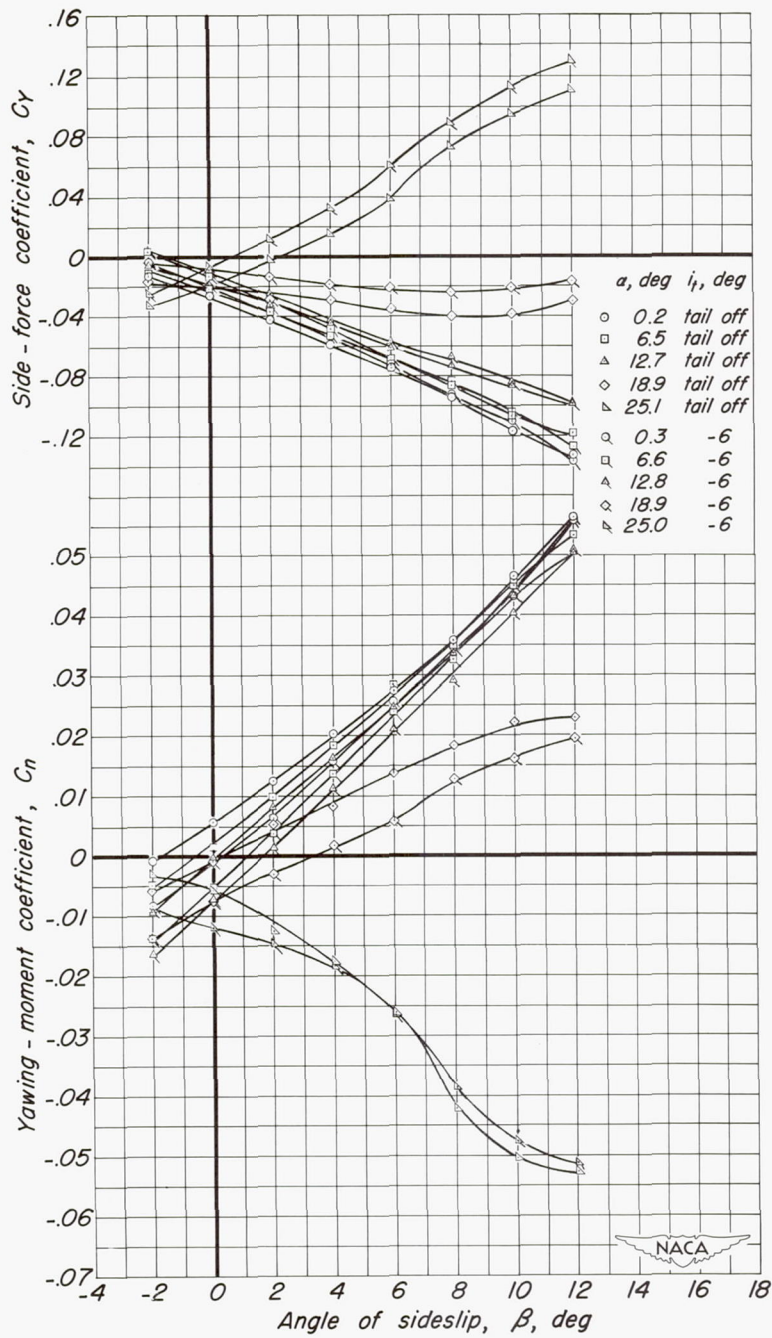
(c) C_Y, C_n vs β

Figure 17.— Concluded.
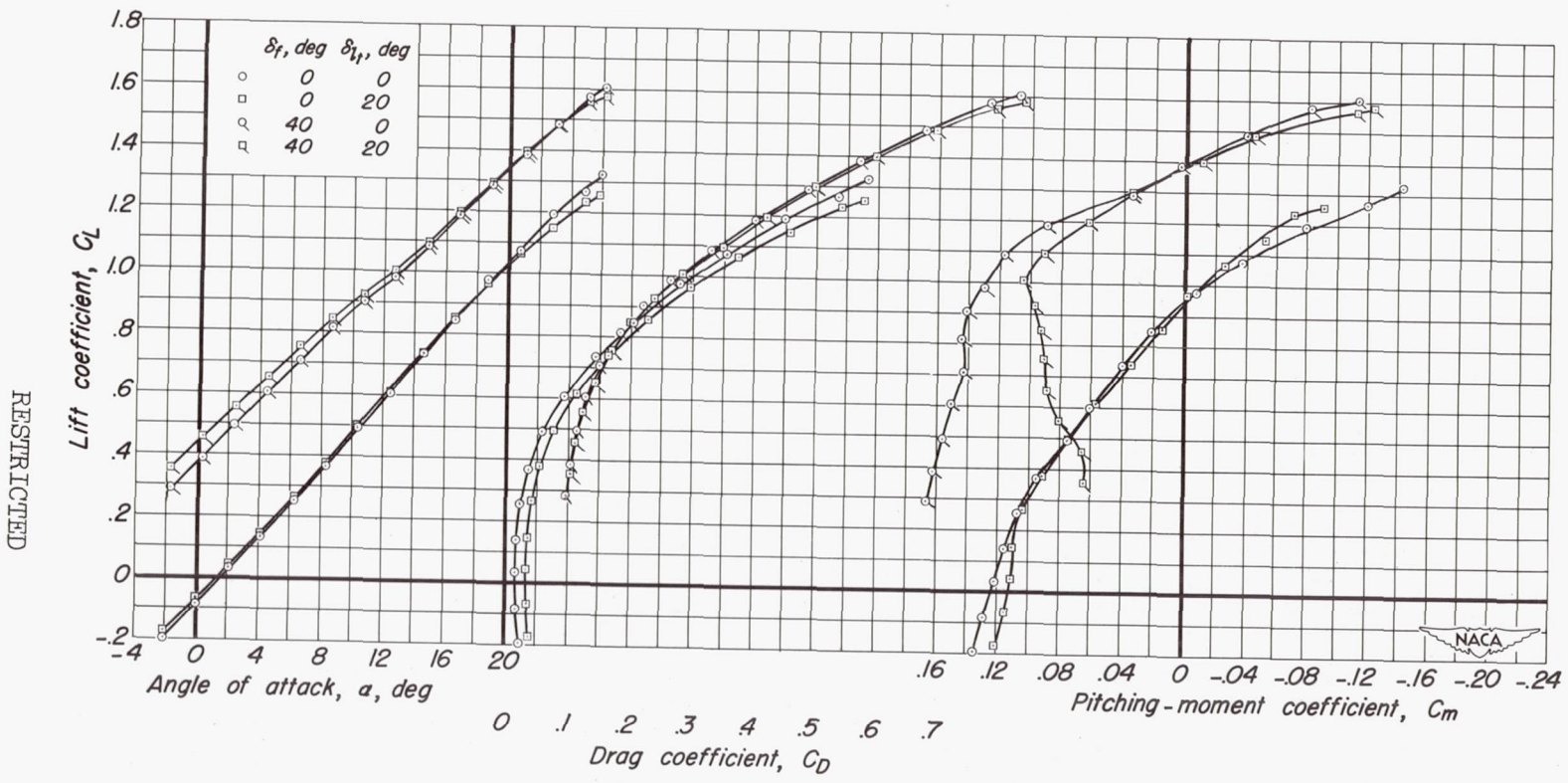
(a) C_L vs α, C_D, C_m

Figure 18.— The effect of flap deflection on the effectiveness of the horizontal tail used as a lateral-control device. $\frac{z}{b/2}$, 0; moment center 0.436 $\bar{c}$; i_t, -6°.
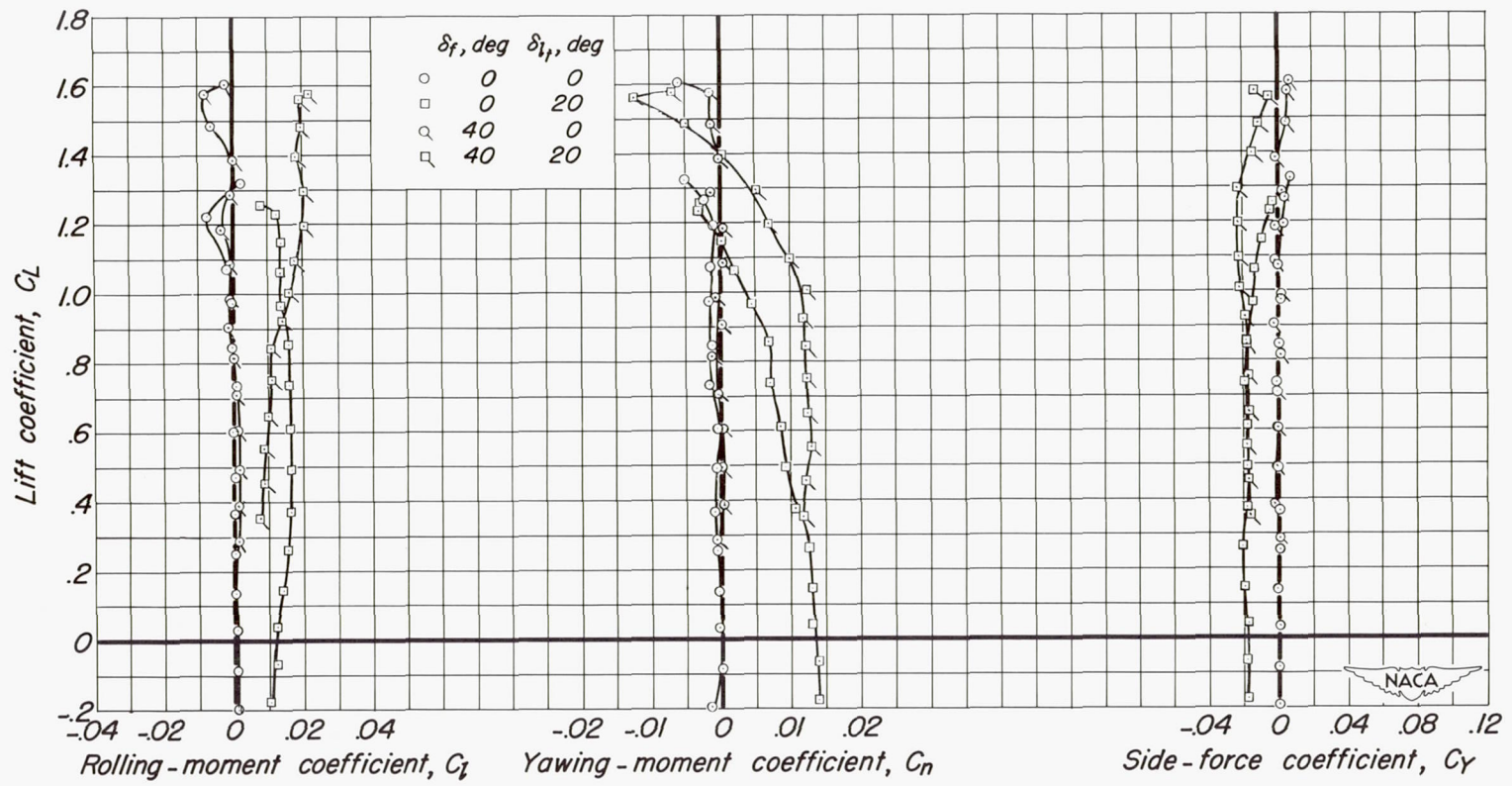
(b) C_L vs C_l , C_n , C_Y

Figure 18.— Concluded.
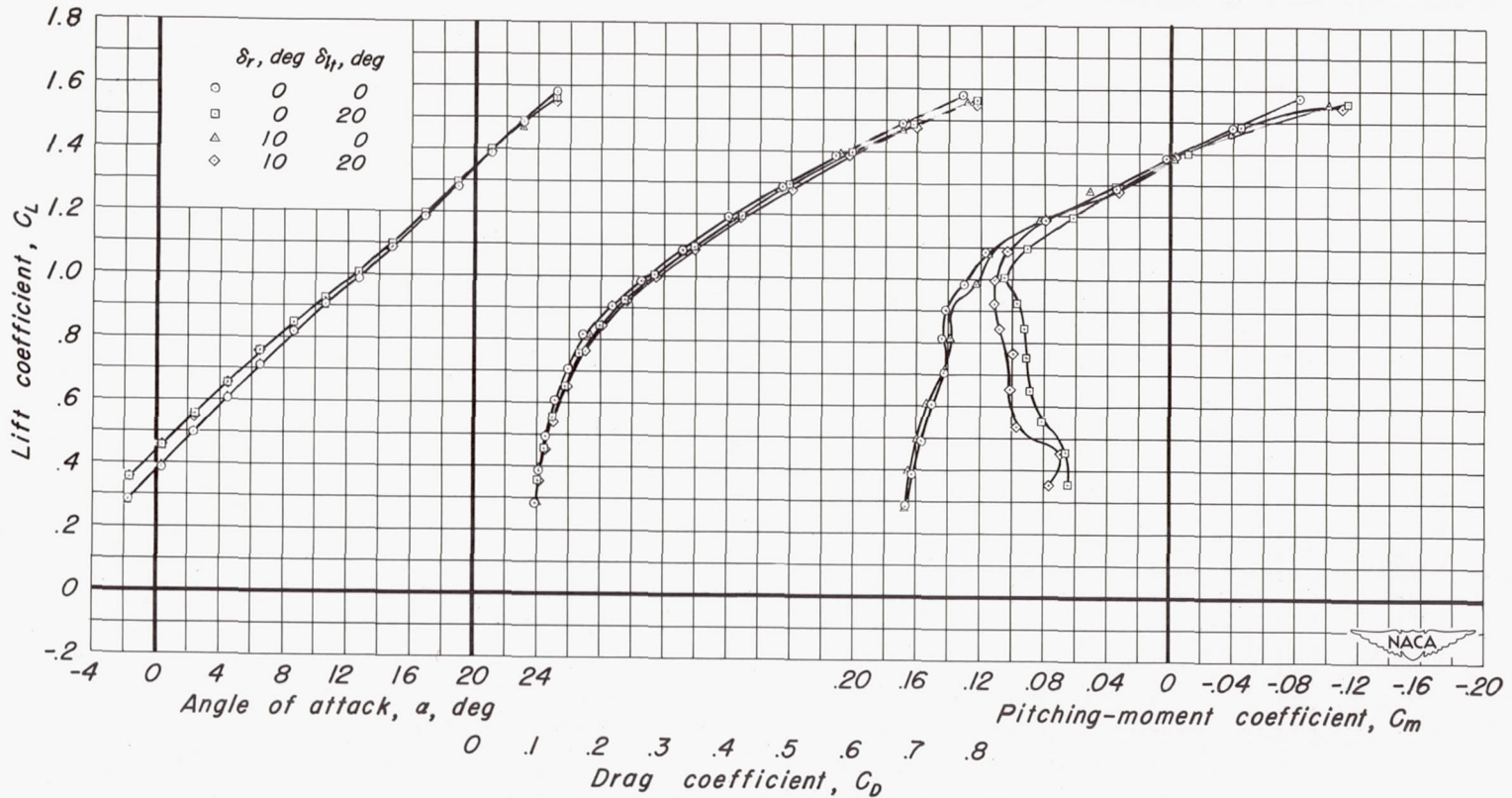
(a) C_L vs a, C_D, C_m

Figure 19.— The effect of rudder deflection on the effectiveness of the horizontal tail used as a lateral - control device. $\frac{z}{b/2}$, 0; moment center $0.436\bar{c}$; δ_f, $40°$; i_t, $-6°$.
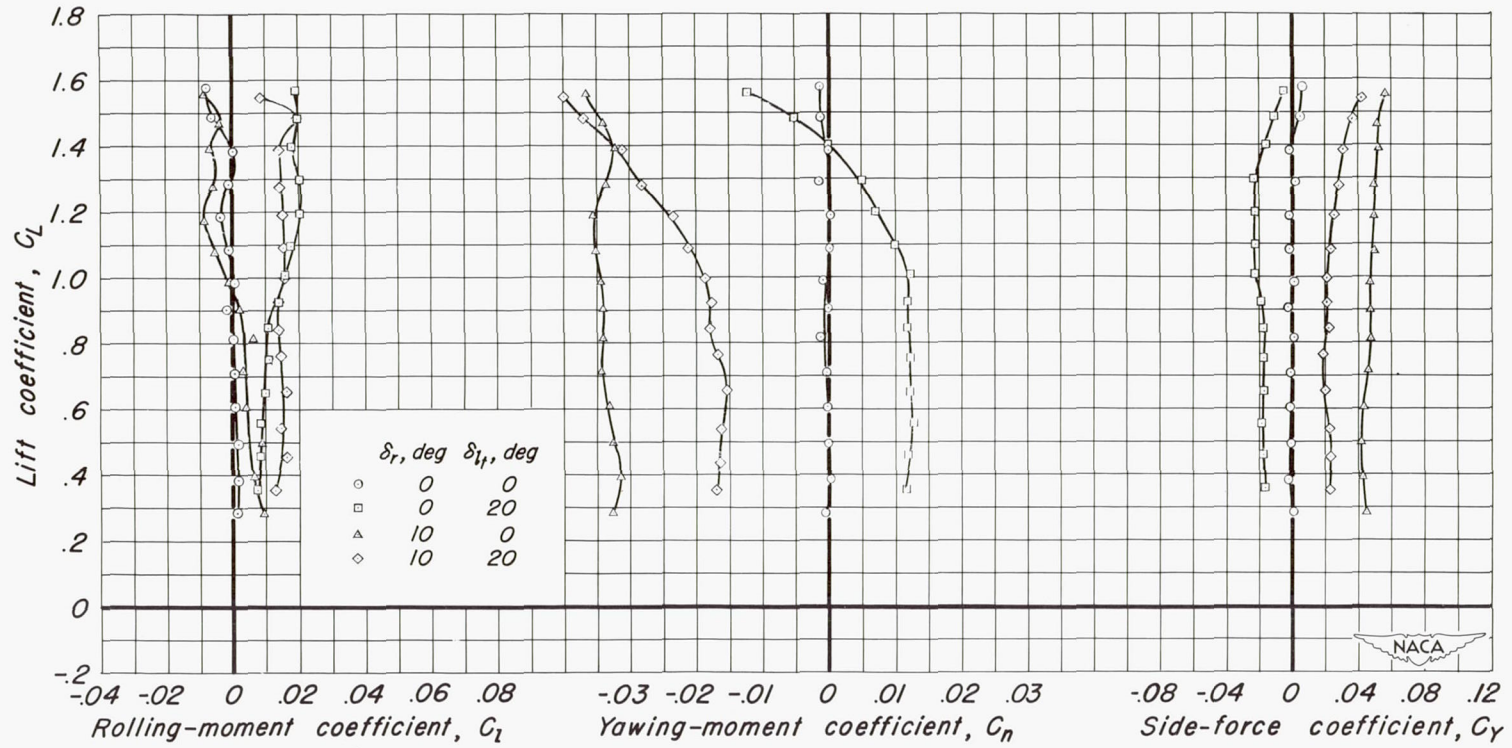
(b) C_L vs C_l , C_n , C_Y

Figure 19.— Concluded.
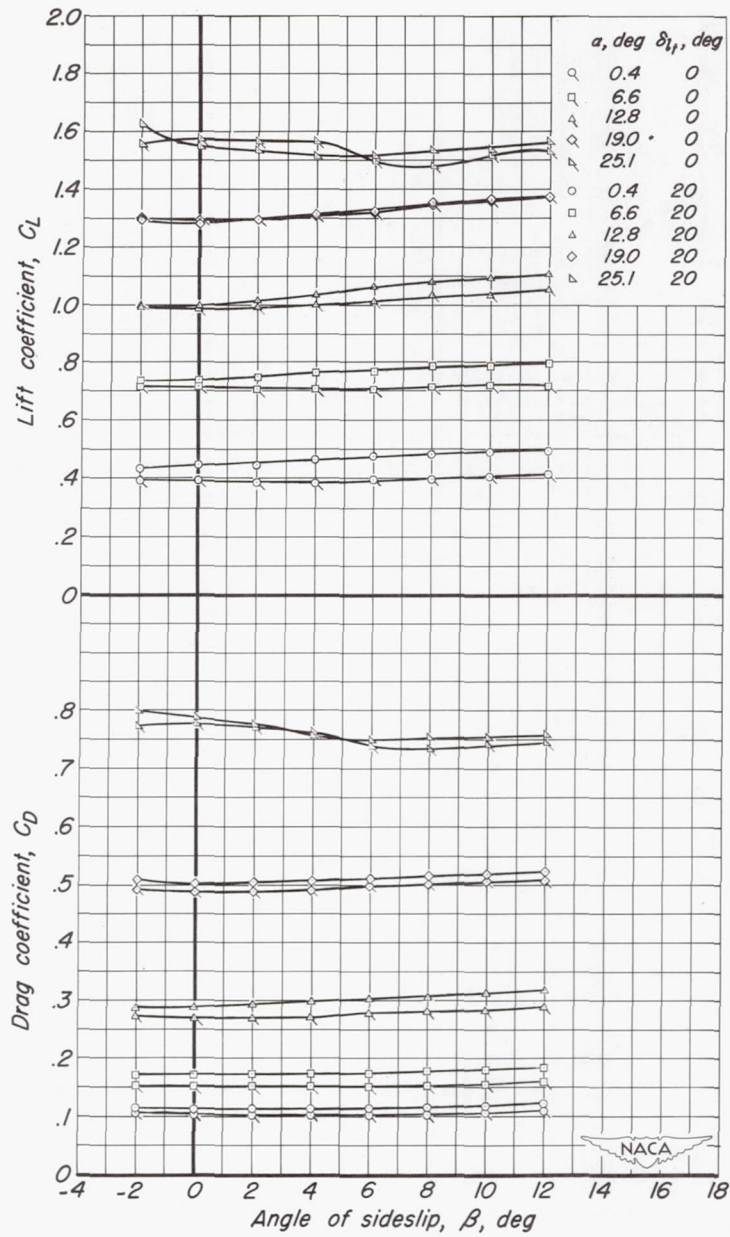
(a) C_L, C_D vs β

Figure 20.— The effect of the horizontal tail used as
a lateral-control device on the characteristics of the
model in sideslip with the rudder deflected 10°.
$\frac{z}{b/2}$, 0; moment center 0.436c̄; δ_f, 40°; i_t, -6°.
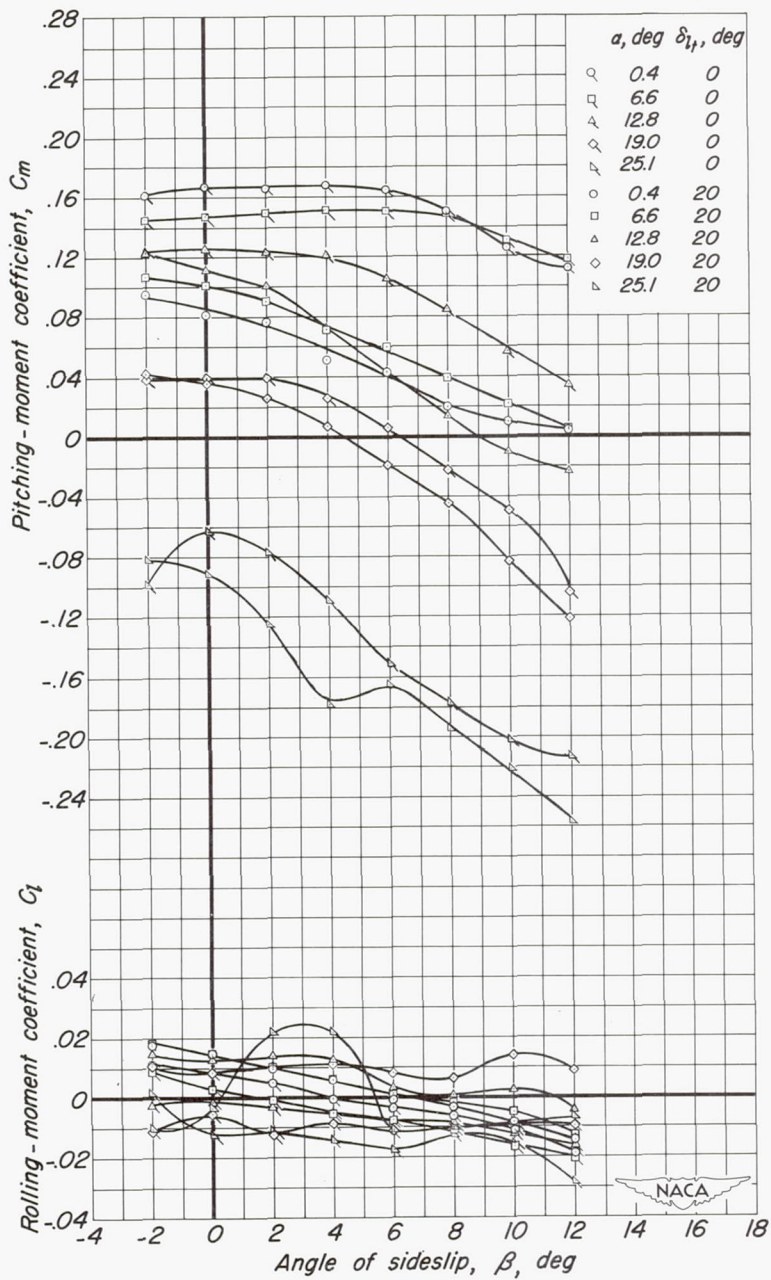
(b) C_m, C_l vs β

Figure 20.– Continued.
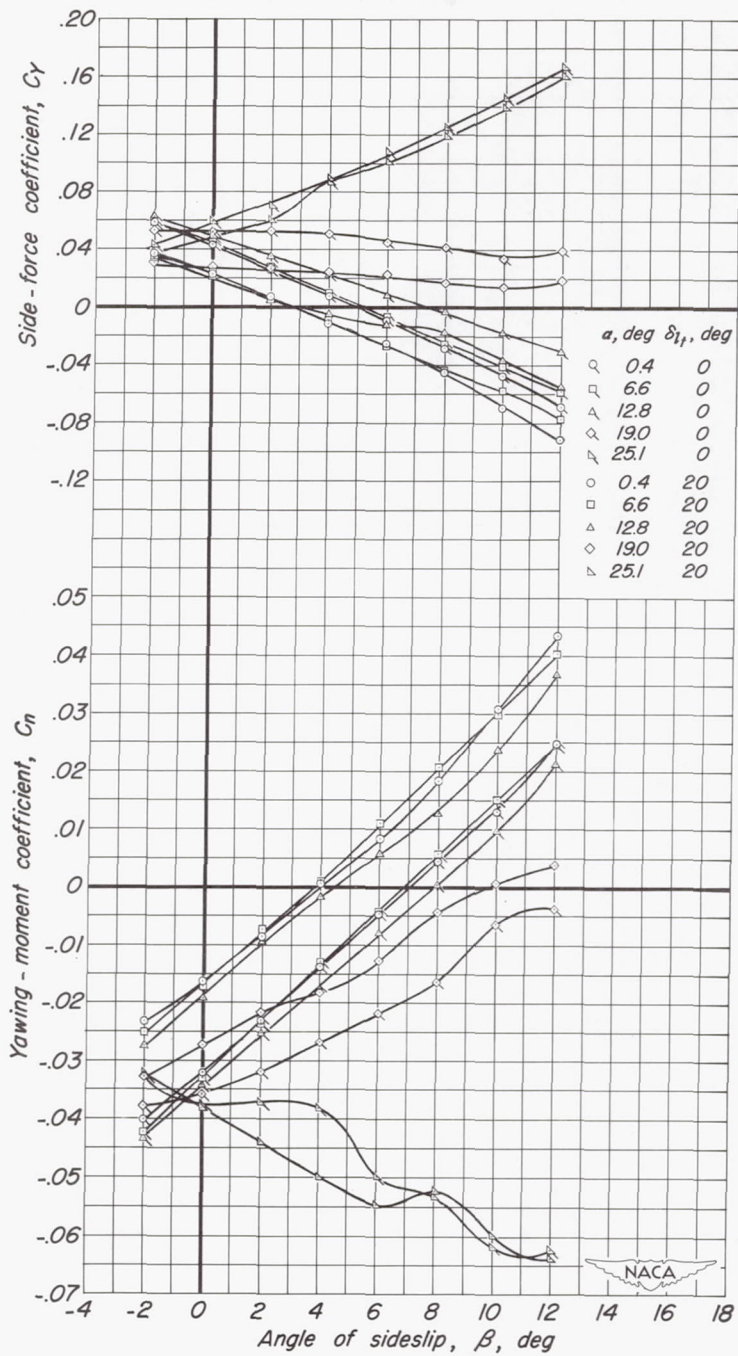
(c) C_Y, C_n vs β

Figure 20.— Concluded.
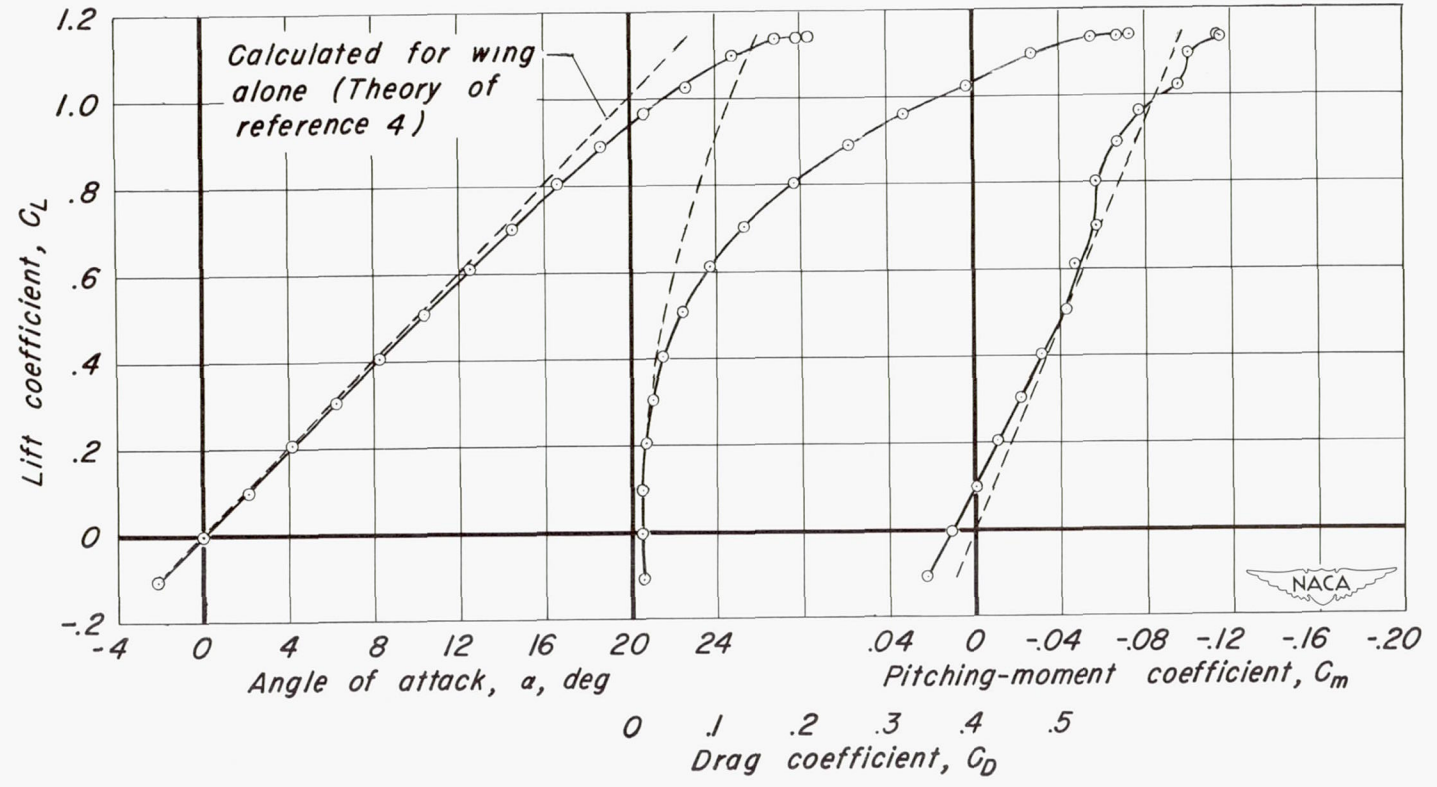
Figure 21.— A comparison of the experimental longitudinal characteristics of the model (horizontal tail off) with those predicted by reference 7. Moment center, 0.250c̄; δ_f, 0°.
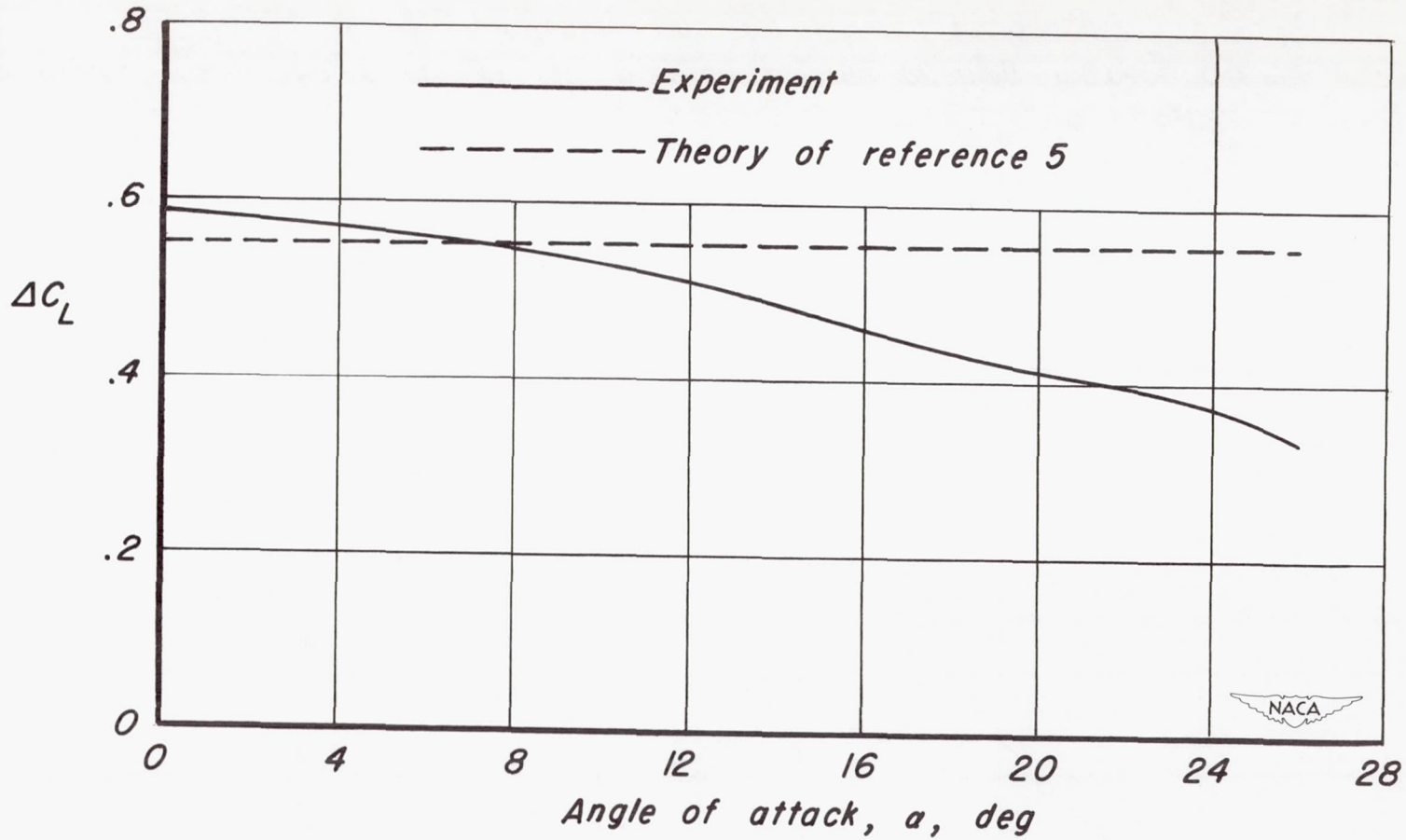
Figure 22.— The lift increment of the model, ΔC_L, obtained by deflecting the flaps to 40°, without the horizontal tail.
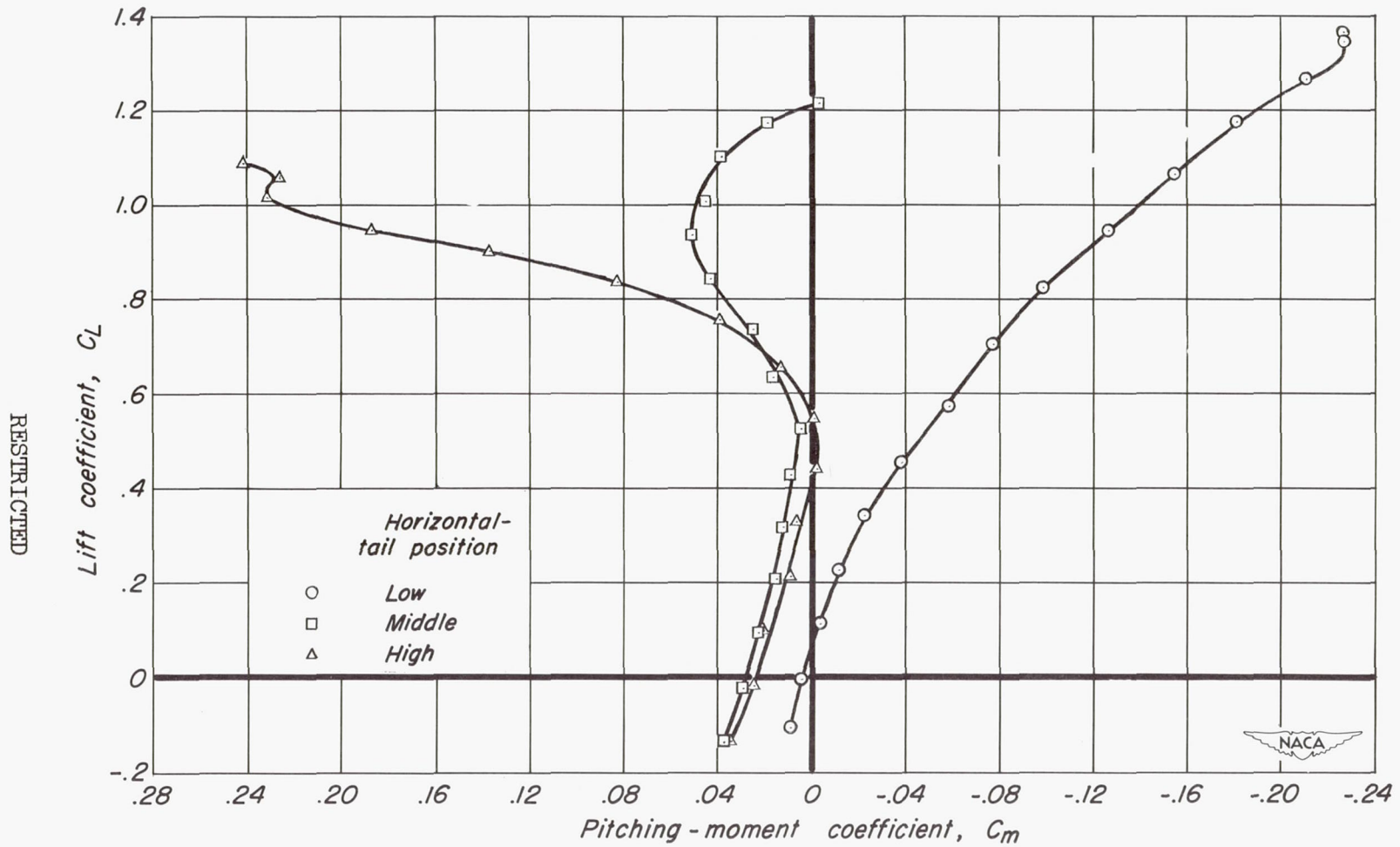
Figure 23.— The effect of tail position on the pitching-moment curves with flaps undeflected and for 0° tail incidence.
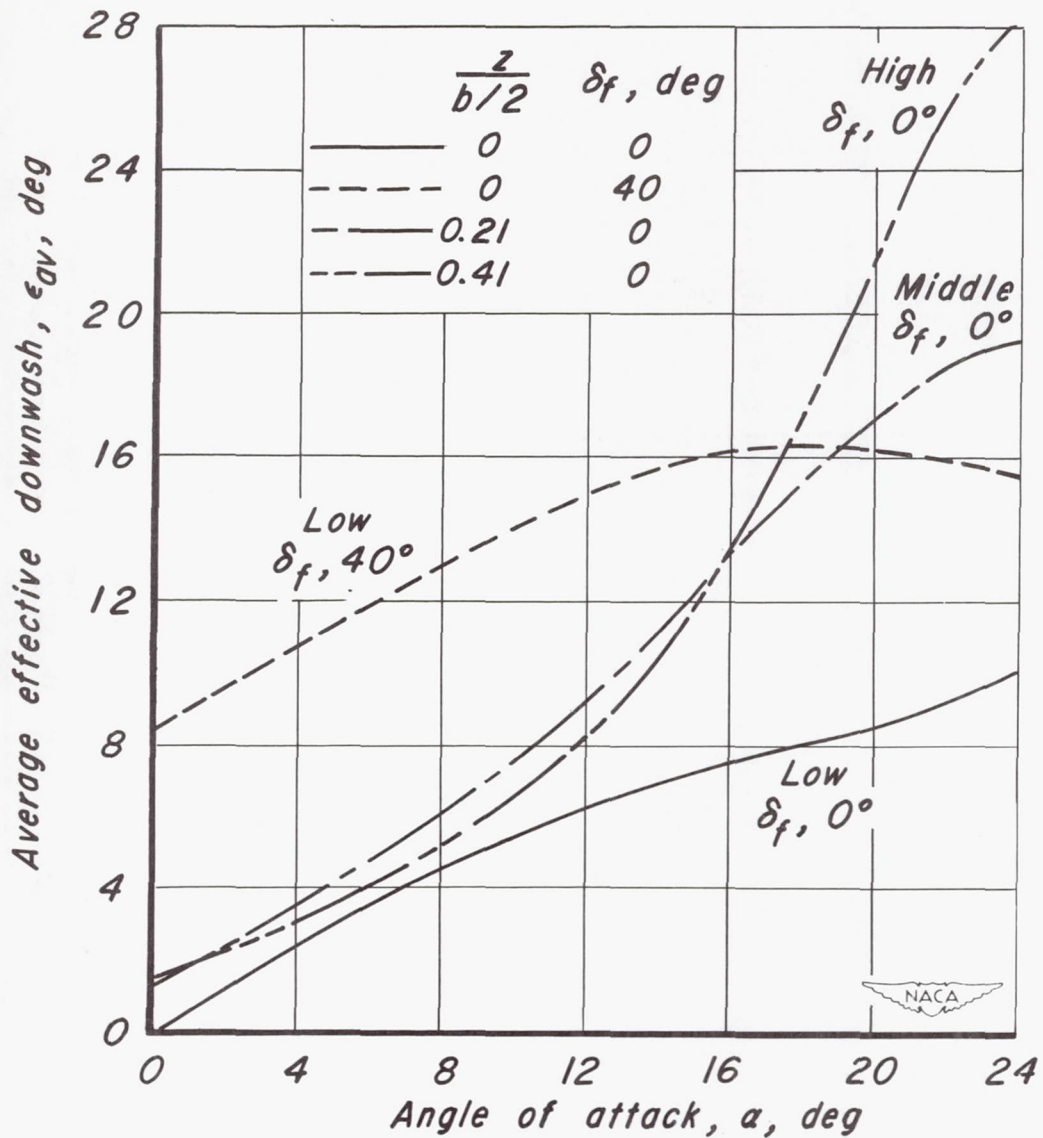
Figure 24.— The average effective downwash at three vertical positions of the horizontal tail.
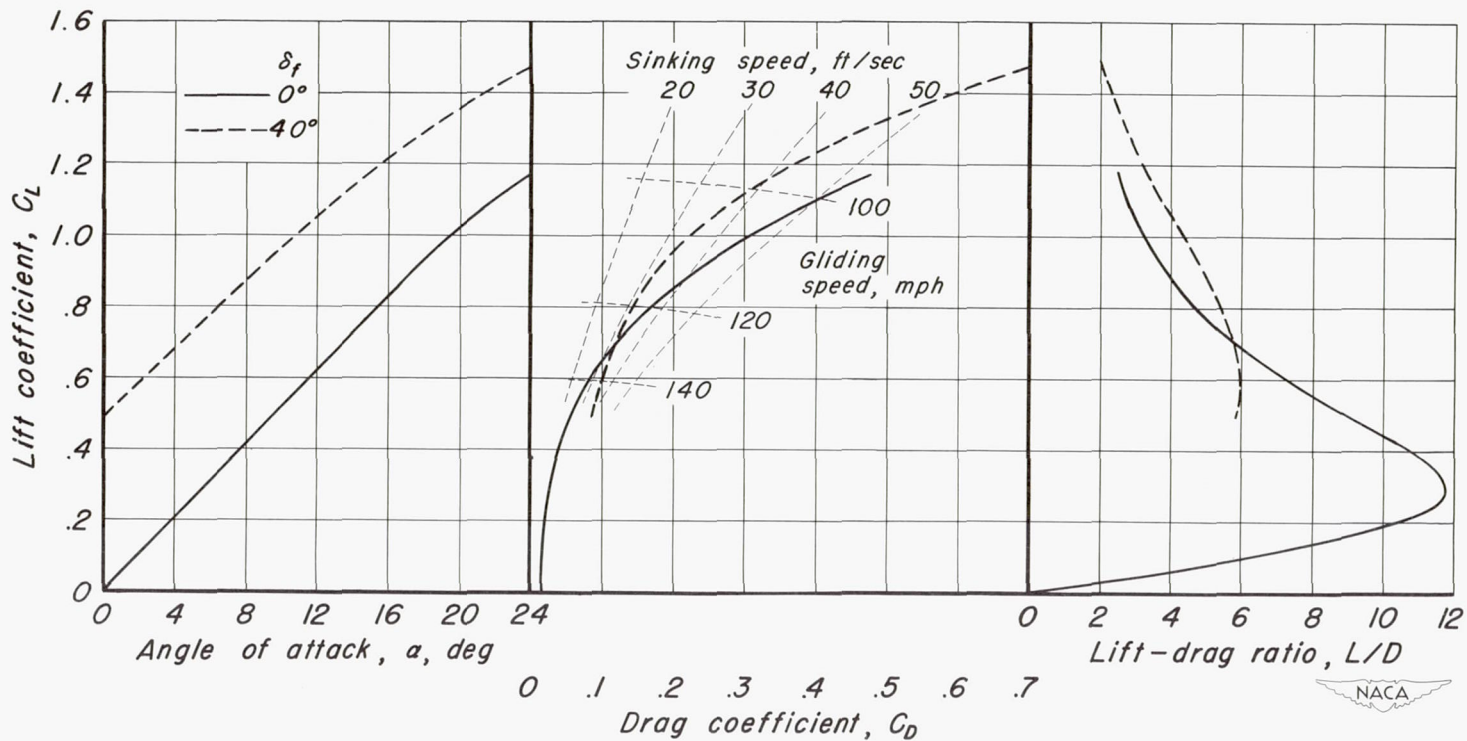
Figure 25.— The effect of flap deflection on the longitudinal trim characteristics of the model with the horizontal tail in the low position. Gliding and sinking speed curves were computed using a wing loading of 30 pounds per square foot.
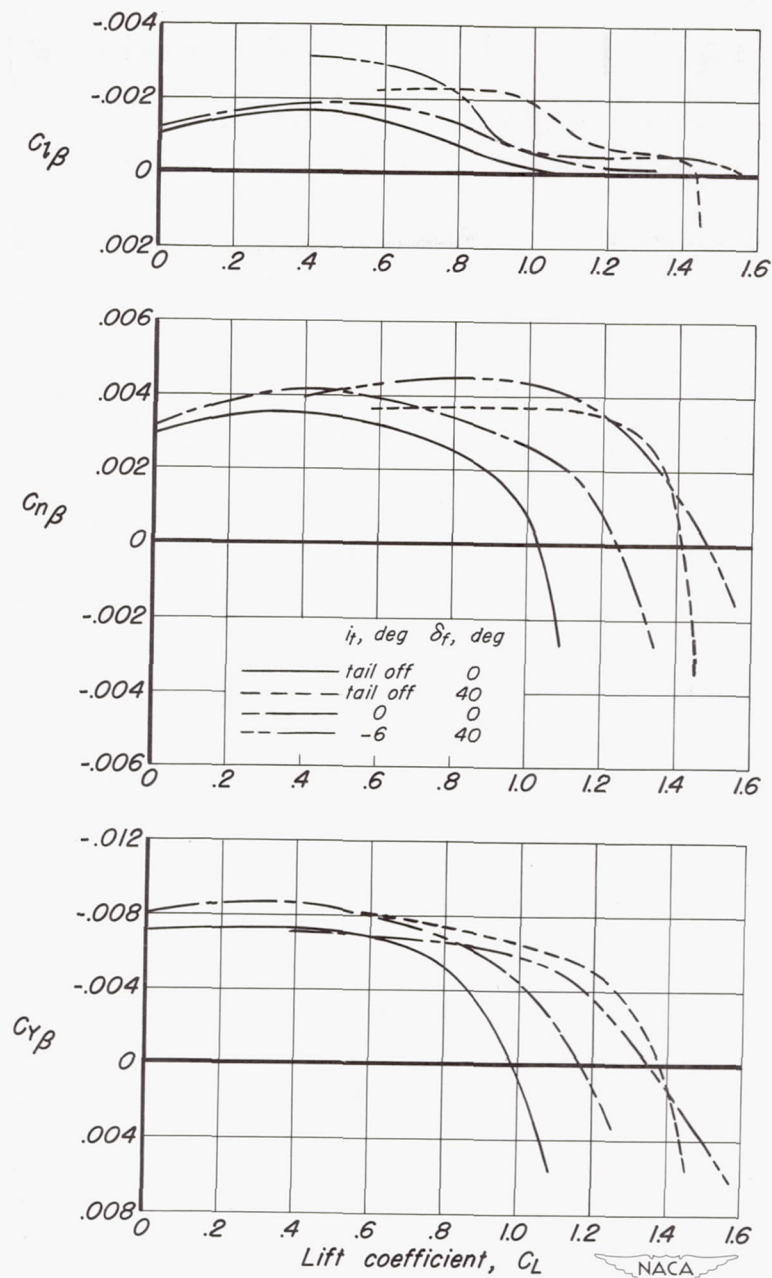
Figure 26.— Sideslip derivatives of the model with and without the horizontal tail, with flaps undeflected and with flaps deflected, 40°.
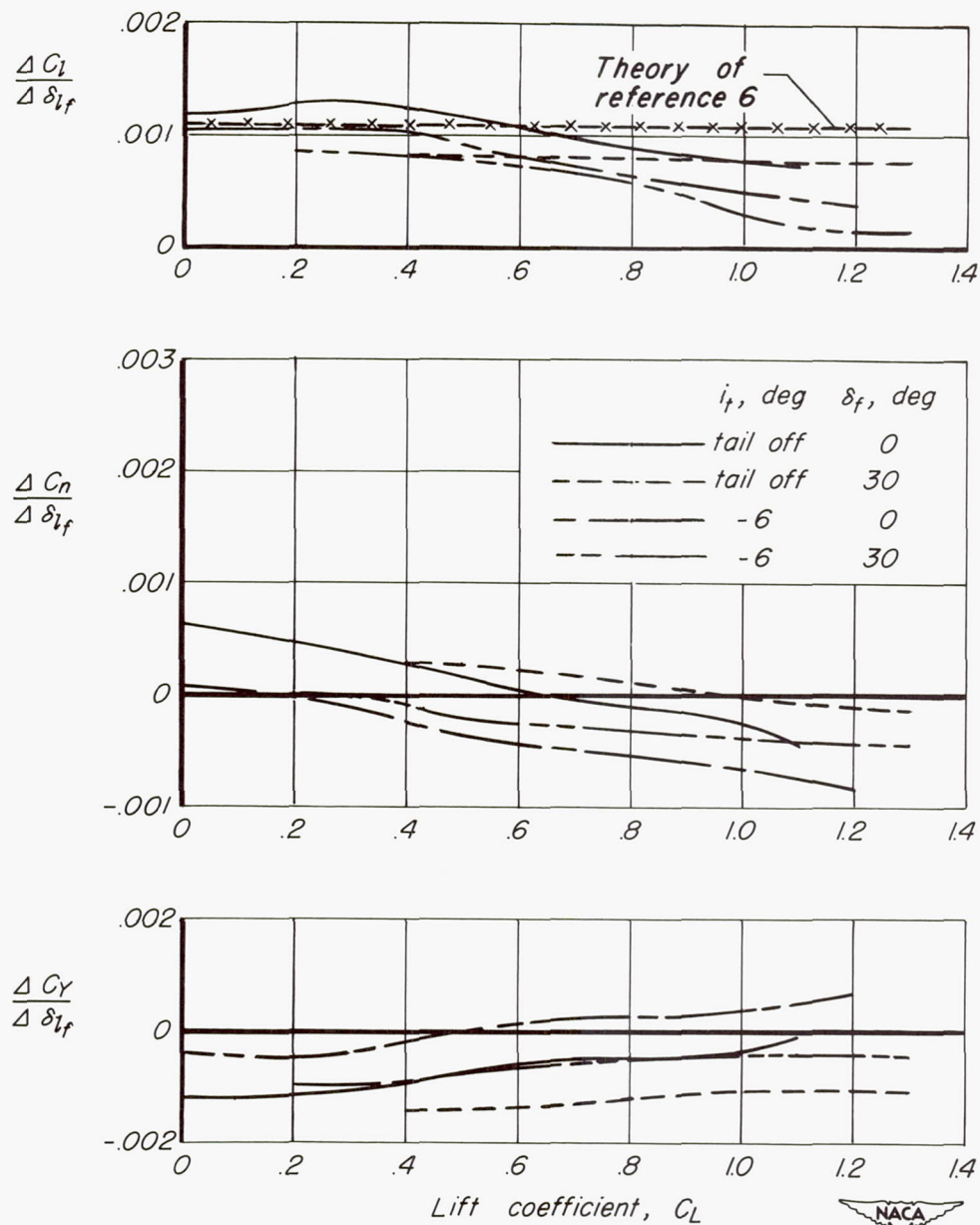
Figure 27.— The increment in rolling moment, yawing moment, and side force per degree of total lateral-control deflection of the flaps. δ_{l_f}, 20°; $\frac{z}{b/2}$, 0.

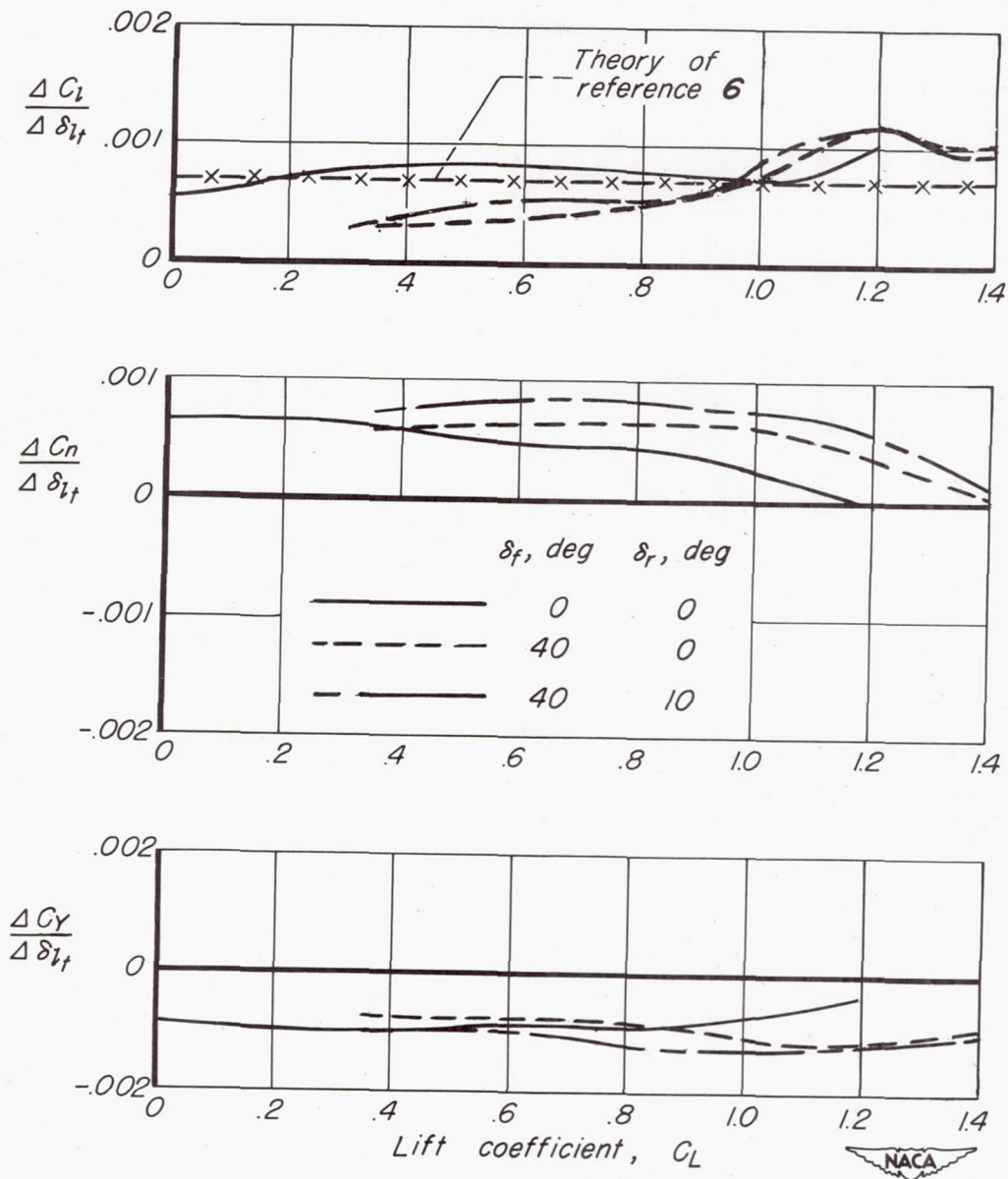Figure 28.— The increment in rolling moment, yawing moment, and side force per degree of total lateral-control deflection of the horizontal tail. δ_{l_t}, 20°; i_t, -6°; $\frac{z}{b/2}$, 0.
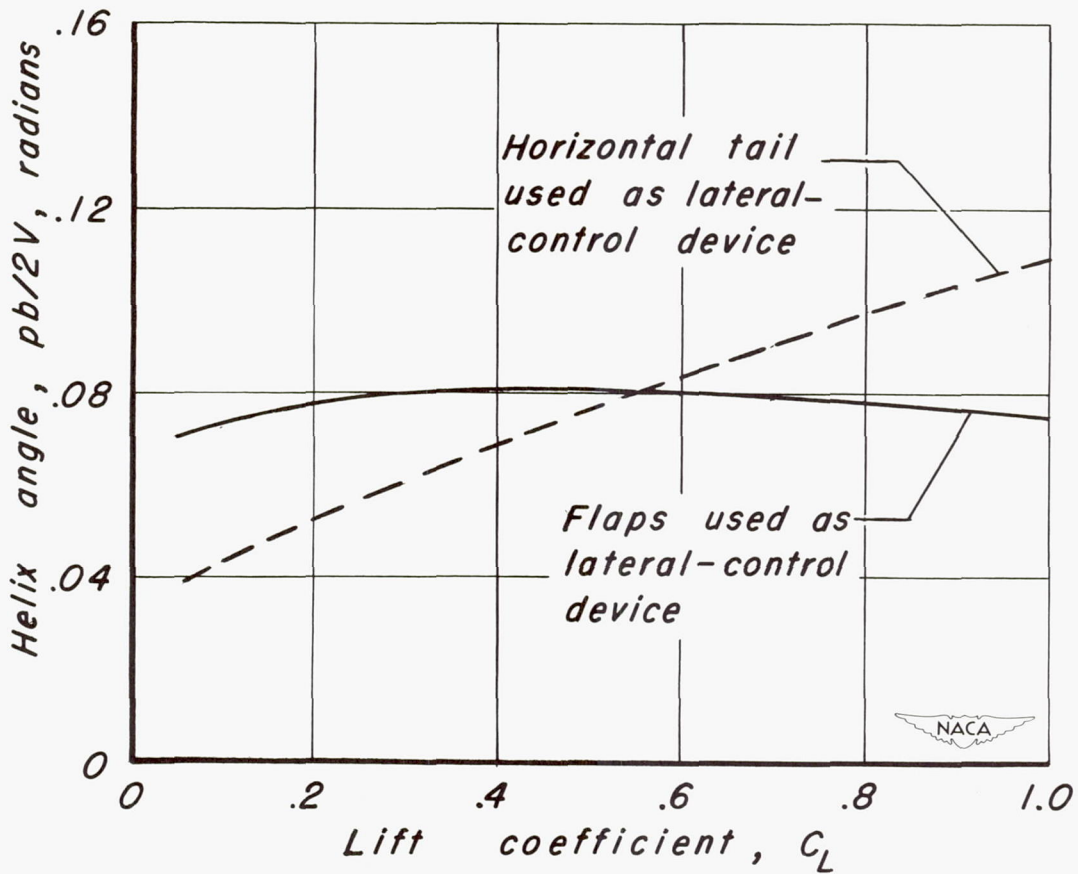
Figure 29.— A comparison of the variation of pb/2V
with lift coefficient for the model with flaps or
horizontal tail used as a lateral-control device.
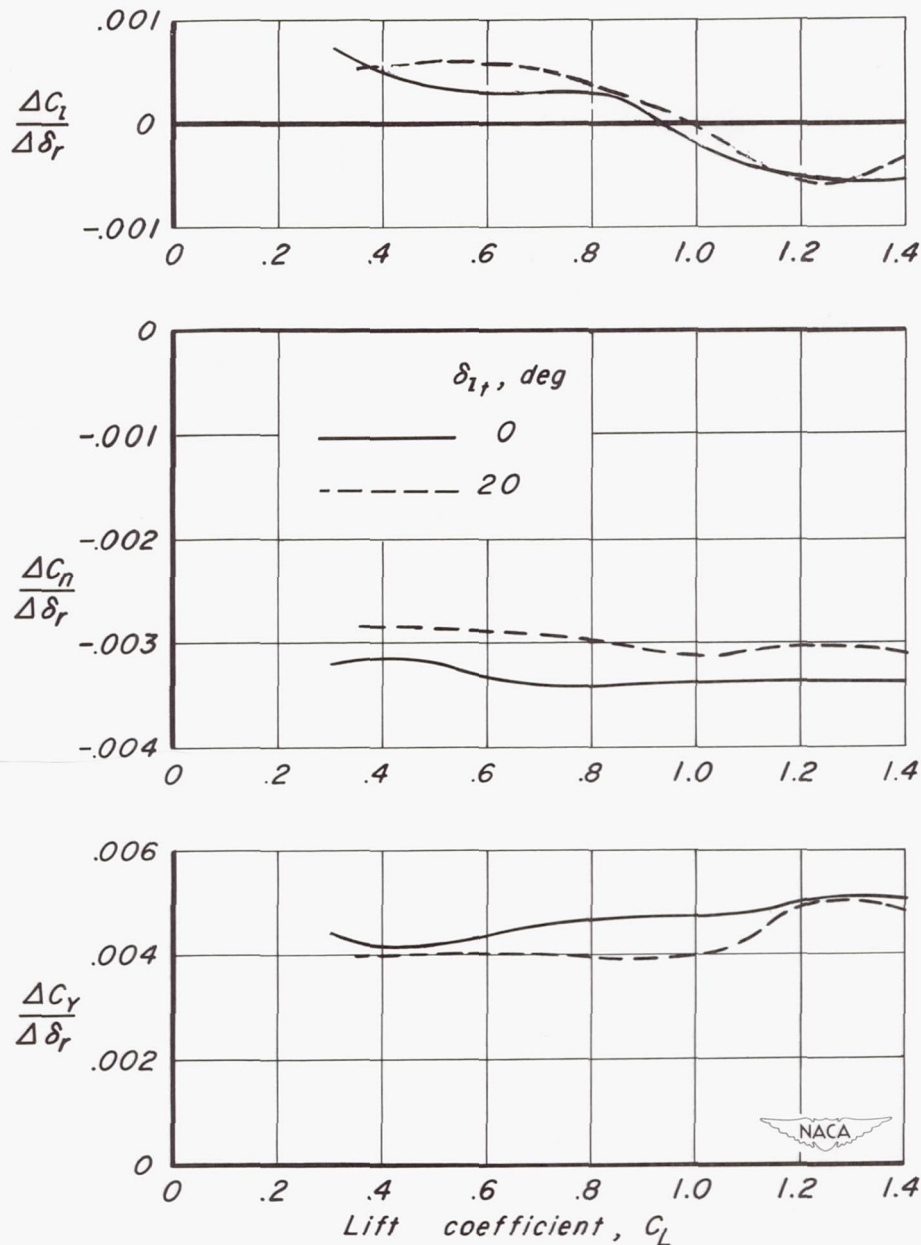δ_l, 10°; i_t, -6°; δ_f, 0°; $\frac{z}{b/2}$, 0.

Figure 30.— The increment in rolling moment, yawing moment, and side force per degree of rudder deflection. δ_f, 40°; i_t, -6°; $\frac{z}{b/2}$, 0.